

MICELLAR CATALYZED REACTIONS
FOR FLOW INJECTION ANALYSIS

BY

MARÍA A. HERNÁNDEZ TORRES

A DISSERTATION PRESENTED TO THE GRADUATE SCHOOL
OF THE UNIVERSITY OF FLORIDA IN
PARTIAL FULFILLMENT OF THE REQUIREMENTS
FOR THE DEGREE OF DOCTOR OF PHILOSOPHY

UNIVERSITY OF FLORIDA

1986

To my parents,
Saúl and Carmen,
with all my love.

ACKNOWLEDGMENTS

I would like to express my gratitude and appreciation to my research director, Dr. John G. Dorsey, for his invaluable assistance, guidance and encouragement throughout the years. I was very lucky to have him as a teacher. His special qualities helped me to develop as a professional, and at the same time he allowed me to grow as an individual. His view of science and life created a good and healthy environment for learning. His lessons will always be remembered.

Special thanks are given to Dr. Morteza G. Khaledi, for his helpful suggestions and advice at the beginning of this project.

I would like to express my gratitude to my colleagues and friends in Dr. Dorsey's research group, for their friendship and daily encouragement. I treasure very much the time spent at the lab with all of them even when life was tough. I will miss them all!

I would like to thank the faculty members at the University of Florida with whom I was in contact during my graduate years. Special thanks are due to the members of my committee, for their contributions to my learning experience.

I would like to mention Cindy Zimmerman, for her promptness and accuracy in typing the final draft of this thesis.

There are no words to express how thankful I am to my family and friends. Their love, support, encouragement, patience, and faith in me made possible this new achievement in my career. I want to thank

my grandparents, Avelina and José Antonio, for their care throughout the years.

TABLE OF CONTENTS

	<u>Page</u>
ACKNOWLEDGMENTS.....	iii
LIST OF TABLES.....	vi
LIST OF FIGURES.....	vii
ABSTRACT.....	ix
CHAPTERS	
I INTRODUCTION.....	1
Principles of Flow Injection Analysis.....	1
Properties of Surfactants and Micelles in Aqueous Solution.....	10
II THEORY AND BACKGROUND.....	17
Chemical Kinetics in a Flow Injection Analysis System....	17
General Features of Micellar Catalysis.....	19
III EXPERIMENTAL: FIA SYSTEM FOR PYRIDOXAL DETERMINATION....	23
Apparatus.....	23
Reagents.....	25
Procedure.....	25
IV MICELLAR CATALYSIS IN THE DETERMINATION OF PYRIDOXAL BY FLOW INJECTION ANALYSIS.....	26
Results and Discussion.....	26
Measurements of Dispersion.....	55
V CONCLUSIONS AND FUTURE WORK.....	70
REFERENCES.....	73
BIOGRAPHICAL SKETCH.....	77

LIST OF TABLES

<u>Table</u>	<u>Page</u>
I Figures of merit for pyridoxal determination.....	40
II Variable parameters for the Modified Simplex Optimization program.....	42
III Optimized and fixed variables for the determination of pyridoxal.....	45
IV Figures of merit for pyridoxal determination with conditions obtained by Modified Simplex program.....	47
V Variance and standard deviation values for pyridoxal in aqueous media at 10% peak height.....	59
VI Variance and standard deviation values for pyridoxal in aqueous media at 30% peak height.....	60
VII Variance and standard deviation values for pyridoxal in aqueous media at 50% peak height.....	61
VIII Variance and standard deviation values for pyridoxal in 0.05 M CTAB micellar media at 10% peak height.....	62
IX Variance and standard deviation values for pyridoxal in 0.05 M CTAB micellar media at 30% peak height.....	63
X Variance and standard deviation values for pyridoxal in 0.05 M CTAB micellar media at 50% peak height.....	64
XI Average values for variance and standard deviation for pyridoxal in 0.05 M CTAB micellar and aqueous media at 10, 30, and 50% peak height for aqueous and 0.05 M CTAB systems.....	65
XII Dispersion values for aqueous and micellar system.....	68
XIII Measurement of dispersion versus CTAB concentration.....	69

LIST OF FIGURES

<u>Figure</u>	<u>Page</u>
1	Diagram of an FIA system (a) and typical recording (b).....3
2	Dispersion in an FIA system.....6
3	Velocity profiles and shapes of injected sample bolus.....9
4	Dill-Flory's representation of a normal micelle.....12
5	A two dimensional schematic representation of the regions of a spherical ionic micelle.....14
6	FIA manifold for the determination of pyridoxal.....24
7	Reaction and surfactant media used for the analysis of pyridoxal.....27
8	Absorbance versus wavelength (nm) in aqueous system for the determination of pyridoxal.....29
9	Absorbance versus wavelength (nm) in 0.05 M CTAB micellar system for the determination of pyridoxal.....30
10	Change in maximum absorbance (355 nm) versus time (minutes) in aqueous media for the determination of pyridoxal.....31
11	Change in maximum absorbance (355 nm) versus time (minutes) in 0.05 M CTAB micellar media for the determination of pyridoxal.....32
12	Log ($A_{\infty}-A_t$) versus time (minutes) for pyridoxal in aqueous system.....34
13	Log ($A_{\infty}-A_t$) versus time (minutes) for pyridoxal in 0.05 M CTAB system.....35
14	Absorbance calibration plots for pyridoxal in aqueous (□) and 0.05 M CTAB (■) systems.....36

15	Fluorescence calibration plots for pyridoxal determination in aqueous (□) and 0.05 M CTAB (■) systems.....	38
16	Absorbance calibration plots for pyridoxal in aqueous (□) and 0.09 M CTAB micellar (●) media.....	46
17	Absorbance recordings of a series of pyridoxal standards in aqueous media.....	48
18	Absorbance recordings of a series of pyridoxal standards in 0.05 M CTAB micellar media.....	49
19	Absorbance recordings of a series of pyridoxal standards in 0.09 M CTAB micellar media.....	51
20	Fluorescence recordings of a series of pyridoxal standards in aqueous media.....	52
21	Fluorescence recordings of a series of pyridoxal standards in 0.05 M CTAB micellar media.....	54
22	Measurement of peak width, W, and asymmetry factor, B/A, at 10, 30 and 50% peak height in an FIA peak.....	57

Abstract of Dissertation Presented to the Graduate School
of the University of Florida in Partial Fulfillment of the
Requirements for the Degree of Doctor of Philosophy

MICELLAR CATALYZED REACTIONS
FOR FLOW INJECTION ANALYSIS

BY

MARÍA A. HERNÁNDEZ TORRES

August, 1986

Chairman: Dr. John G. Dorsey
Major Department: Chemistry

In this study, the applicability of micellar carrier streams for the catalysis of reactions in FIA was investigated. Flow Injection Analysis (FIA) is an automated kinetic method of analysis. An FIA system with low dispersion and fast reaction kinetics will provide low limits of detection and high sampling rates.

Micelles exhibit the ability to solubilize hydrophobic compounds on or within their structures. The rate of many reactions in micellar media is altered due to the proximity of reagents and analyte, changes in the microenvironment and orientation of solutes.

The advantages of combining the solubilization property and micellar catalysis for a given reaction that is taking place in an FIA system are demonstrated. The reaction of pyridoxal (a B₆ vitamer) with cyanide was investigated in aqueous and micellar media. The cationic surfactant, hexadecyltrimethylammonium bromide (CTAB), was chosen for the micellar carrier solution. The oxidation product of

this reaction, 4-pyridoxolactone, was detected either fluorimetrically or by ultraviolet absorbance. The reaction rates in the two media were determined and compared. Calibration plots for pyridoxal were made and the analytical figures of merit were compared for aqueous and 0.05 M CTAB micellar media.

A Simplex Optimization was carried out for the determination of pyridoxal in micellar media. A new set of conditions for micellar media was obtained from the Simplex program. With this new set of conditions, a calibration plot for the micellar media was prepared and subsequently compared to the calibration plot for the aqueous system. The analytical figures of merit for the two carrier solutions were calculated and compared.

The peak shape obtained in the FIA system was investigated. The standard deviation and variance at 10, 30, and 50% peak height were calculated by empirical equations. The agreement of these values allows the peaks to be classified as exponentially modified gaussians.

Measurement of dispersion in both aqueous and micellar systems was investigated. Dispersion values for both aqueous and micellar systems were examined by two methods: by using the definition of dispersion in FIA and by measuring the variance (second moment) at 10% peak height. In both methods, higher values for dispersion were obtained for micellar media.

CHAPTER I INTRODUCTION

Principles of Flow Injection Analysis

Flow injection analysis (FIA) is now established as a fast, precise, accurate, efficient and extremely versatile analytical tool. The FIA technique is used by many analytical chemists working in a variety of different industries and institutions (1-9).

A historical review of the development of FIA reveals that since its conception in the early 1970s, many of the concepts of flow injection analysis have been adopted from other fields and many workers have contributed to its development (10). However, the technique of FIA became known by the simultaneous appearance of the work of Stewart, Beecher and Hare (11) in the United States and Ruzicka and Hansen (12) in Denmark in 1975. The Danish group developed the method using primarily instrumentation normally associated with segmented flow analyzers. In contrast, the American group based their initial work on high performance liquid chromatography components. For this reason, FIA is considered a hybrid of the two techniques.

In the past, it was generally assumed based on Skegg's concept that air segmentation and attainment of a steady state signal were essential for performing continuous flow analysis (6). The presence of air bubbles in the analytical stream was thought to be necessary

to limit sample dispersion, to promote mixing of the sample with reagents (by generating turbulent flow) and to scrub the walls of the analytical conduits to prevent carryover of samples. However, it was proven that analysis without air segmentation is not only possible but also advantageous. In FIA, there is no air segmentation, the sample is introduced as a plug via a valve or syringe, mixing is mainly by diffusion-controlled processes, and the response curves do not reach the steady-state plateau, but have the form of sharp peaks. The absence of air segmentation leads to a higher sample throughput. The presence of a sample carrier interface over which concentration gradients develop during the course of analysis has opened new analytical possibilities for continuous flow analysis. The reproducibility is good, and there is no sample carryover. There is no need to introduce and remove air bubbles, and an expensive high quality pump is not necessary.

Flow injection analysis is based on the injection of a liquid sample into a moving, nonsegmented reagent carrier stream. The injected sample forms a zone that disperses and reacts with the carrier on its way to a detector (5). The simplest FIA analyzer (Figure 1a) consists of a pump (P) that propels the carrier stream (R), an injector port (S), by which a well defined sample volume is injected into a carrier stream, and a coil in which the sample zone disperses and reacts with the components of the carrier stream, forming a species to be sensed by a flow-through detector (D). A typical recording has the form of a sharp peak (Figure 1b) the height of which is related to the concentration of analyte, and the time from

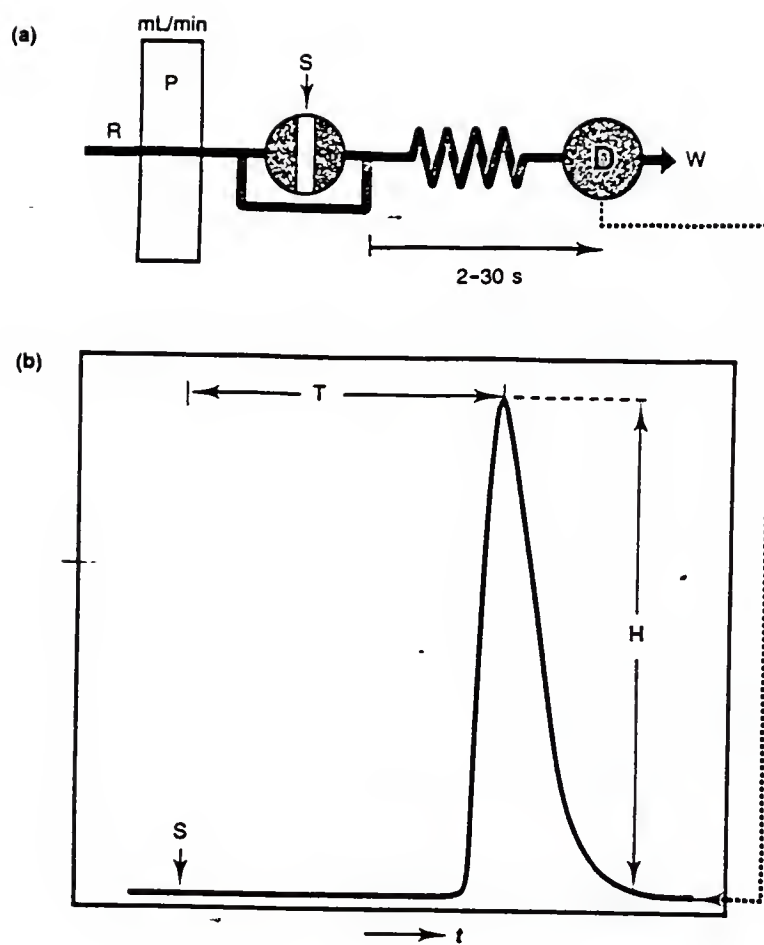


Figure 1. Diagram of an FIA system (a) and typical recording (b) (from 1).

injection to peak maxima is termed the residence time. Residence times are typically from 3 to 30 seconds.

Between the points of injection and detection the sample plug will have been physically dispersed to some degree and, in addition, some chemical reactions will have taken place. The peak will reflect both processes.

The injection of a sample has to be done in such a way that by inserting a discrete slug of sample into a continuously moving stream the movement of the stream is not disturbed. The residence time of the sample in the analytical manifold should ideally be identical for each sample, and the conditions to which the sample is exposed during processing should also be the same. The reason for this is that not only the physical dispersion but the chemistry involved requires a reproducible travel pattern of the sample from the point of injection to detection. In an FIA system, neither the mixing nor the chemical reaction is complete; an equilibrium for either process is not attained (1). By monitoring the reaction at a fixed precise time, the concept of the steady state can be abandoned. This measurement at a fixed time is just as analytically significant as the steady state signal. Any fluctuations in residence time of the sample, i.e., variation in flow rate, will result in imprecise measurement of the signal.

When a sample is first injected, it forms a well-defined sample plug in the stream. As the sample is swept downstream through the analytical conduits of narrow bore tubing, the plug disperses into and, thus, mixes with the carrier stream under laminar flow conditions

to form a gradient. The magnitude of this dispersion is dependent on the operating parameters applied to the system, including sample volume, tubing bore size, tubing length, flow rate, sample volume and coil diameter (1,6). Varying the values of these parameters confers a significant degree of control over the dispersion characteristics and facilitates optimization of a flow injection system for many diverse applications, so that the optimum response is obtained at minimum time and reagent expense.

The response curve has the shape of a peak reflecting a continuum of concentrations. In contrast to all previous methods of automated assay, there is no single element of fluid that has the same concentration as the neighboring one (7) (Figure 2).

The dispersion coefficient, D , is the ratio of the concentration of sample solution before (C^0) and after (C) the dispersion process has taken place (Figure 2). The dispersion coefficient can be defined at any point of the curve but, for convenience in the majority of FIA methods, the dispersion coefficient is defined at maximum peak height.

$$D = \frac{C^0}{C^{\max}} \quad (\text{eq. 1.1})$$

In cases where a reaction is developed as a result of mixing effected by dispersion, the peak height will increase as the reaction proceeds toward completion. The maximum response will then be attained when an optimum balance is reached between dispersion and reaction time.

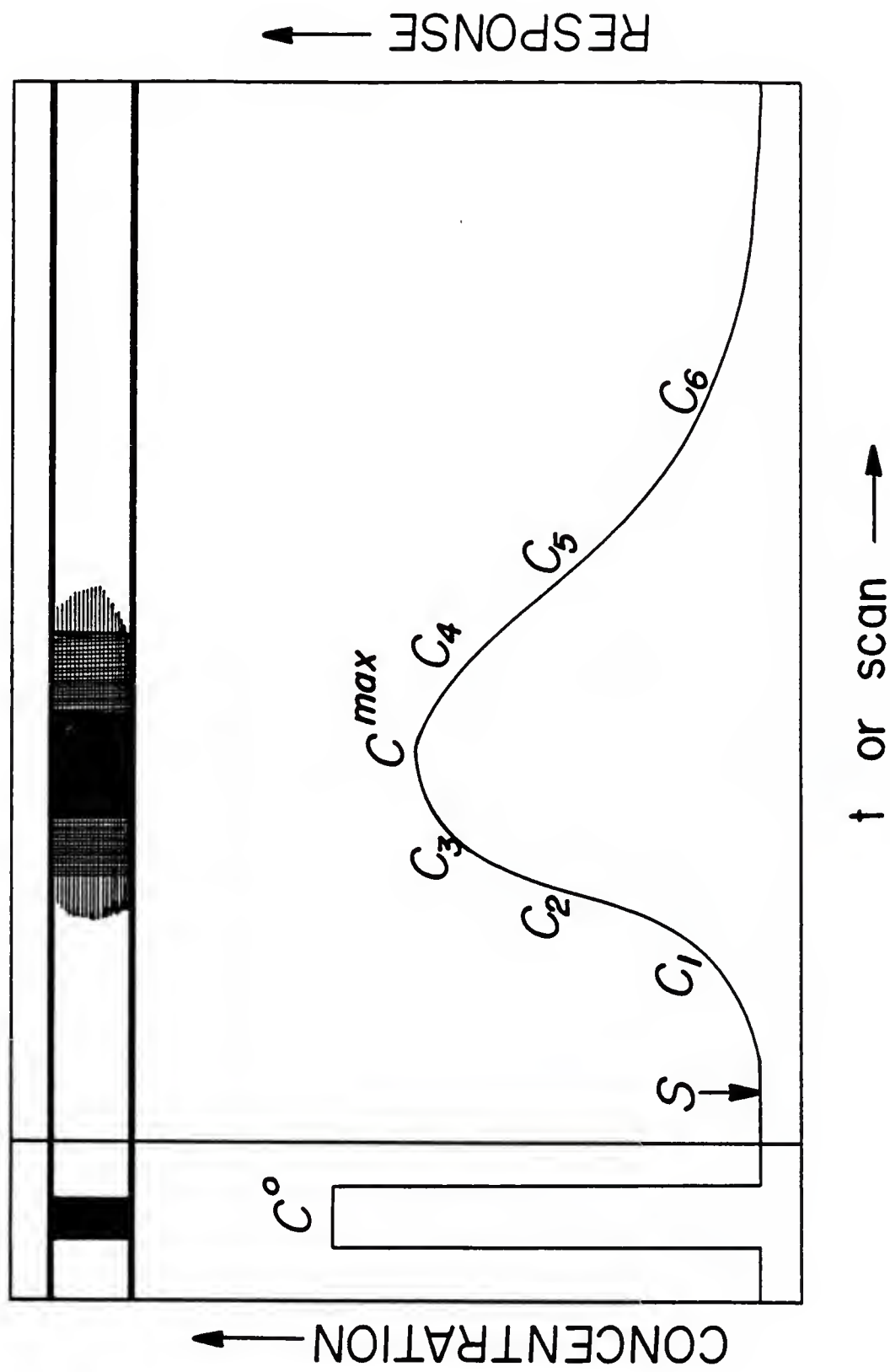
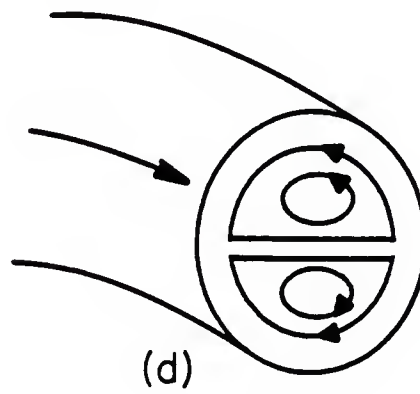
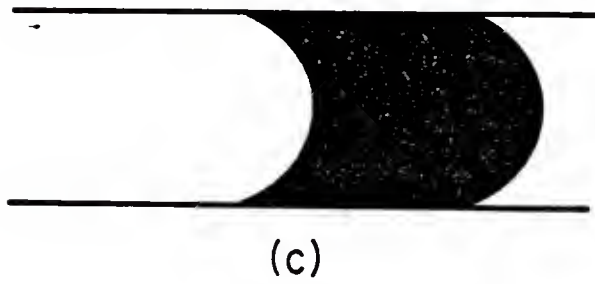
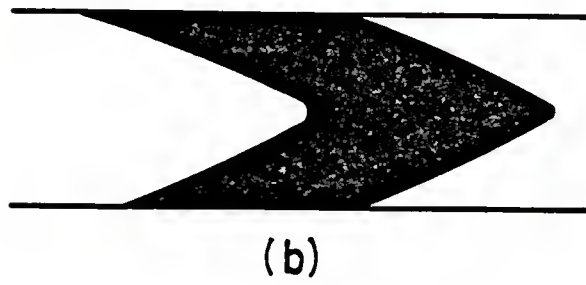
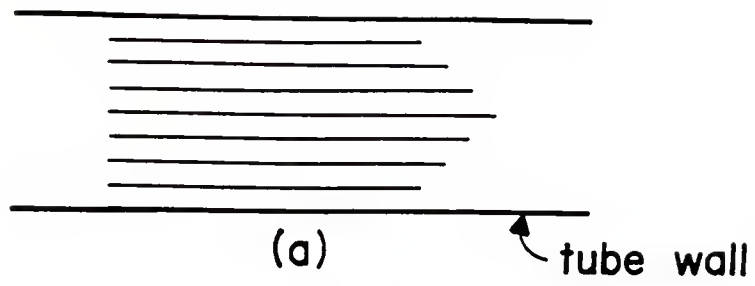


Figure 2. Dispersion in an FIA system (from 7).

Flow injection analysis operates only in the laminar flow region (3,13-16). In this region, FIA systems generate dispersion through both diffusion and convection. Under such conditions of laminar flow, the layer of liquid in contact with the tube surface is practically stationary and the velocity of centrally placed molecules is twice the mean velocity of the liquid. This gives rise to a parabolic velocity profile (Figure 3a). In the absence of molecular diffusion, a sample placed into a moving stream would have an infinitely long tail by the time it reached the detector (Figure 3b). This results in unacceptable carryover between samples. Diffusion of molecules between the carrier and sample bolus serves to limit this convective dispersion and effectively mixes sample and reagent. In coiled tubes, it is the radial rather than the axial dispersion that contributes most significantly to sample dispersion in FIA systems. This type of dispersion, also called secondary flow, operates to move the fluid both toward and away from the tubing wall and thus serves as an efficient scrubbing mechanism (Figure 3d). A molecule located at the center will tend to diffuse into a region of lower sample concentration and by doing so it will move into a layer of liquid moving at a slower longitudinal velocity. On the other hand, a molecule located near the wall will diffuse toward the center of the carrier solution and it will encounter a layer of faster moving liquid, which will carry it away from the wall and toward the center of the sample zone. This radial diffusion perpendicular to the direction of the flow modifies the shape of the bolus head and the result is low carryover and cross contamination. High sample

Figure 3. Velocity profiles and shape of an injected sample bolus:
(a) Laminar flow, parabolic velocity profile; (b) Sample dispersion caused by laminar flow without diffusion; (c) Sample shape resulting from laminar flow with molecular diffusion; (d) Secondary flow pattern in the cross-section of a tightly coiled tube (from 3).



throughput is obtained because of the limited band spreading. When samples under these conditions reach the detector they have a shape as in Figure 3c.

The versatility and simplicity of FIA systems permits this technique to be widely used for performing chemical assays. The recent increase in publications dealing with new FIA methods as well as in separate symposia on this topic indicate the popularity of this relatively new technique (2). On the other hand, more has to be done on the theoretical side, where the dispersion of the sample zone must be investigated in much greater detail. The theory of dispersion, although very useful, is far from being exact and complete (17). Only deeper theoretical studies will lead to design of even more advanced continuous flow techniques that will allow chemical analyses to be performed in new ways.

Properties of Surfactants and Micelles in Aqueous Solution

Scientists from around the world have shown special interest in surfactants because of their unique characteristics (18-24).

Surfactants, or surface active agents, are amphiphilic molecules having both pronounced hydrophobic and hydrophilic properties.

Surfactants are classified as cationic, anionic, nonionic or zwitterionic according to the hydrophilic part (polar head group).

The hydrophobic tail consists of a hydrocarbon chain usually from 8 to 20 carbon atoms in length. Furthermore, this hydrophobic tail can contain unsaturated portions or aromatic moieties, can be partly or

completely halogenated, and can be branched or consist of two or more chains.

At low concentration, the surfactant is dispersed predominantly as monomers, although dimers, trimers, etc. can exist. Over a narrow concentration range, termed the critical micelle concentration (CMC), surfactants have the important property of forming molecular aggregates, called micelles. Above the CMC, there exists a dynamic equilibrium between monomers and micelles. The amount of free monomer remains approximately constant and equal to the CMC.

In aqueous solutions, surfactant molecules (typically from 60 to 100) associate to form a roughly spherical cluster (25) (Figure 4). This micelle structure is such that the hydrophilic head groups are directed toward and in contact with the aqueous solution, forming a polar surface, while the hydrophobic tails are directed away from the water forming a liquid-like hydrocarbon core. The microviscosity of this core is considerably higher than in hydrocarbons. The micellar surface is not uniform: some of the hydrocarbon chains are turned towards the solvent or at least come into contact with it periodically (26). On the whole, it may be supposed that the micellar surface is a polar environment differing in properties from water itself.

Changes in temperature, concentration of surfactant, additives in the liquid phase, and structural groups in the surfactant may cause changes in the size, shape, and aggregation number of the micelle (26-28).

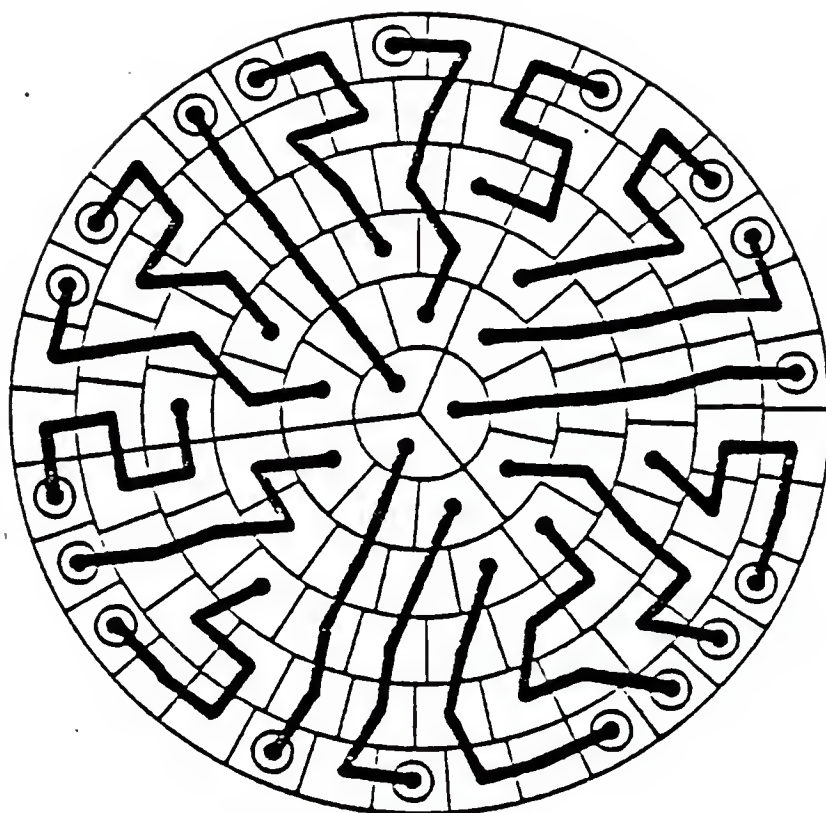


Figure 4. Dill-Flory's representation of a normal micelle. The ionic head groups are indicated by the circles, and the hydrocarbon chains are pointing toward the center of the micelle (from 25).

In micelles of ionic surfactants, the charged head groups and the counterions are located in a compact region, known as the Stern layer, which extends from the core to within a few angstroms of the shear surface of the micelle. Beyond the Stern layer, the remainder of the counterions are located in the Gouy-Chapman electrical double layer where they are completely dissociated from the charged aggregate and are able to exchange with ions in the bulk of the solution (26) (Figure 5).

The driving force for micelle formation in aqueous media is due primarily to the hydrophobic effect, and the electrostatic repulsion between the ionic head group limits the size that a micelle can attain, thereby keeping the micelle size small.

One of the most important properties of micellar systems is their ability to solubilize a variety of species (18-24,26-28). Solubilization may be defined as the spontaneous dissolving of substance (solid, liquid or gas) by reversible interaction with the micelles of a surfactant in a solvent to form a thermodynamically stable isotropic solution with reduced thermodynamic activity of the solubilized material (24). The importance of the phenomenon of solubilization from the practical point of view is that it makes possible the dissolving of substances in solvents in which they are normally insoluble or slightly soluble. Solubilization is a dynamic equilibrium process and depends on temperature, nature of solute, surfactant concentration and type of micellar system employed (26). There are several possible solubilization sites and orientations available in a micellar system and the site occupied by a solubilize

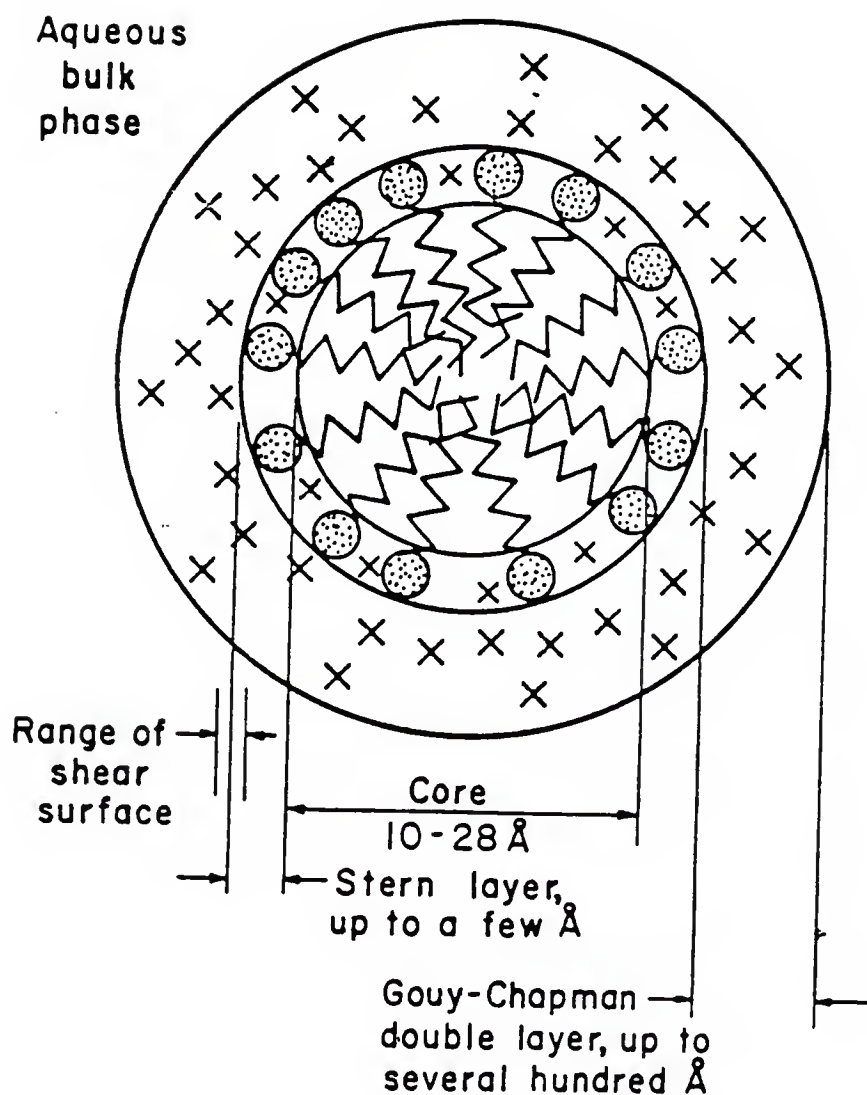


Figure 5. A two dimensional schematic representation of the regions of a spherical ionic micelle (from 24).

depends upon the nature of both the solute and the micelle. There is a rapid equilibrium between various possible sites and also between the solubilized state and the free state in the aqueous medium. The site of solubilization is a topic of current debate. Some contend, if the solute is nonpolar, it may pass completely into the hydrophobic core or penetrate a particular depth into the surface layer. Others contend it may be adsorbed at a hydrophobic region on the surface (18).

Micellar systems are very useful in the field of analytical chemistry due to the unique properties of these organized assemblies. Micelles can lead to the modification and improvement of existing procedures and to the development of new methods of chemical analysis. Micellar structures offer means to overcome solubility problems, to speed reaction rates of analytical reactions and to reduce side reactions, to shift acid base or redox equilibria, to change spectral distribution or intensities, and to improve selectivity and efficiency in extraction and chromatographic methods. Several reviews on the use of surfactants in analytical chemistry have appeared (29-31).

Our studies are directed mainly to observing the behavior of combining micellar media with the technique of FIA. This represents the first attempt to demonstrate the advantages of combining the solubilization property and micellar catalysis for a given reaction that is taking place in an FIA system. Higher sensitivity and/or lower limits of detection are expected for a given FIA system when the reaction is carried out with the appropriate micellar media. Kinetic

studies and measurement of the analytical figures of merit will be compared for reactions taking place in aqueous and micellar media.

CHAPTER II THEORY AND BACKGROUND

Chemical Kinetics in a Flow Injection Analysis System

It is well recognized that flow injection analysis yields a response curve which is the result of two processes, both kinetic in nature: the physical process of dispersion and the chemical process of formation of reaction products (1-6,32).

The kinetics of physical dispersion, or incomplete mixing, has been described in a number of papers (14-16,33-35) while attempts to describe the effect of chemical kinetics has been practically ignored. The shape of the transient peak profiles of FIA determinations have been described only in terms of the dispersion process. However, there has been an attempt recently to explore in more detail the complexity of the overall kinetic process taking place inside the sample plug and its boundaries in FIA systems and the contribution of this kinetic chemistry to the peak profiles. Ruzicka and Hansen recognized that "it is obvious that the comprehensive theory of the flow method will eventually combine the theory of mixing of liquids in continuous moving streams with the theory of chemical kinetics" (36). From now on, more attention will be paid to the chemistry process that is taking place (37-42).

In developing a flow injection method, one of the primary goals is to maximize response together with sample throughput. These

parameters are intimately related to the sensitivity of the method and the number of injections possible per hour.

Since there exists an interdependence between the reaction rate and the rate of dispersion, both factors have to be weighed when designing a new FIA system. The longer a sample stays within the system, the greater will be the signal due to the chemistry that is taking place. Longer residence times mean more time is allowed for the reaction to take place, therefore more product is formed. This increase is balanced against the point where dispersion will overcome the formation of the product and cause the signal to decrease. The longer the sample stays between the points of injection and detection, the higher will be the dispersion and the signal measured (usually peak height) will decrease. Another factor to be considered is time needed for each determination. Longer residence times allow maximum sensitivity of measurement but at the expense of decreasing sample throughput. Therefore, short residence times are often preferred.

Fast chemical reactions are required for performing a simple FIA analysis at a continuous carrier pumping rate with practical residence times of about 30 seconds. Slow reactions must presently be performed by the stopped flow mode or in a packed reactor (17). In stopped flow mode, an electronic timer is used to cease the movement of the carrier stream containing the sample zone in order to allow enough time to produce an adequate amount of detectable product, and then the sample is pumped through the flow cell while the peak is recorded in the usual manner. Reactors packed with inert materials, such as glass,

enhance micromixing of sample and reagents in the carrier stream without loss of peak height or loss of sample frequency.

General Features of Micellar Catalysis

It has been reported that with the proper choice of surfactant the rate of a chemical reaction is substantially enhanced in a micellar solution relative to that in the corresponding aqueous system (18,24,26,27,31,43-45).

Research on the effect of surfactants on the kinetics of organic reactions has demonstrated that it is the micelle structure, not the individual molecules, that is responsible for the catalysis or inhibition of these reactions. In accordance with this fact, the term micellar catalysis has been applied to this phenomenon. Rate acceleration or inhibition of organic reactions in micellar solution arises from different rates of reaction of the substrate in the micellar phase and in the bulk solution and the distribution of the substrate between these two phases (26,32). Then, a prerequisite to understanding reaction kinetics in micellar systems is to understand the structure and solubilization properties of the micelles themselves (vide supra).

The kinetics of organic reactions occurring in micellar systems are dominated by electrostatic and hydrophobic interactions between the micelle structures, reactants, transition states and products.

The two physicochemical factors responsible for the efficiency of micellar catalysis are

(1) the change in the reactivity of reagents on transfer from water to the micellar phase and

(2) the concentration of reactants into the micellar phase.

The first factor, the differences in reactivity, can be explained by the difference in the distribution of a substrate between these two phases and by the difference in the degree and nature of substrate-micelle binding. When a solute is solubilized in a micellar system, the microenvironment about it is very different compared to that in the bulk solvent. Micellar systems have the ability to change the effective microenvironment and the microscopic properties of solubilized solutes to that of aqueous media favoring the acceleration of some organic and inorganic reactions.

For catalysis to occur, it is necessary that the substrate be solubilized by the micelle and the site of solubilization be such that the reactive site of the substrate is accessible to the attacking reagent. It is here that hydrophobic interactions become important, because they determine the extent and the site of solubilization in the micelle. In general micellar effects on reactions follow several rules, although there are exceptions. A hydrophobic reactant is attached to a micelle by hydrophobic interactions, independently of the charge on the micelle. If the second reactant is oppositely charged to the micelle, it will be bound to the micelle and the reaction is usually accelerated. When micelles and reactant ions bear like charges, the reaction is inhibited due to the repulsion forces between the ions and the micelle's surface. Nonionic or zwitterionic micelles, generally, have no significant influence on the rates of

these reactions. The rate of certain organic reactions is unaffected when one of the reactants is incorporated into the micellar phase and the other is excluded from it. Exceptions to these rules can be explained by the fact that sometimes hydrophobic effects overcome the electrostatic repulsions and even when the micelle's surface charge does not favor the reaction, catalysis does occur.

The orientation of the reagents in micellar media is different from the bulk aqueous phase due to the different microenvironment that the reagents experience on or within the micelles. If this microenvironment is more attractive to reagents, the reagents are going to spend more time on this phase; therefore, they will be concentrated in this region. Also, the micelle structure provides a very specific and reduced region where the reagents are being solubilized. If the reagents are localized within this small region, they are being concentrated and are closer to each other inducing the reaction to go faster. These are called proximity and concentration effects.

Quite generally, increasing the hydrophobic character of the surfactant, having longer alkyl chains, increases its efficiency as a catalyst. At equal concentration of two surfactants, the more hydrophobic may appear to be the better catalyst (or inhibitor) simply because it has greater affinity for the substrate. Variation in substrate structure has a profound influence, in many cases, on the magnitude of micellar catalysis. The general rule seems to be that the more hydrophobic the substrate, the more pronounced the micellar catalysis.

The multiphase profile of surfactant concentration on the reaction rate is as follows: below the CMC, the rate constants are independent of surfactant concentration; above the CMC, the rate constants rise rapidly with increasing surfactant concentration, level off, and finally decrease with increasing concentration of surfactant. This profile can be rationalized by the fact that the rate constant increases as the concentration of micellar bound reactants increases, but eventually an increase in surfactant concentration dilutes the reactants in the micellar pseudophase, with a decrease in the rate constant (18).

The influence of electrolytes on micellar catalysis is less predictable. For most reactions micellar catalysis is inhibited by counterions and the larger the ion, the greater the effect. This behavior has been rationalized by assuming a competition between the reactant and the electrolyte for a binding site on or in the micelle. This salt inhibition may be explained principally by the displacement of one reactant from the micellar surface by the electrolyte. Enhancement of the micellar catalyzed reaction rate by counterions has been suggested to be due to changes in micellar structure by the salts and this new configuration of the surfactants promotes the reactions.

Another advantage of using micellar media is that of favorable substrate partitioning and binding in specific orientations and configurations on the micelle structure. This makes the reaction very selective to that substrate by decreasing the probability of other interfering species competing for the place of the substrate.

CHAPTER III EXPERIMENTAL: FIA SYSTEMS FOR PYRIDOXAL DETERMINATION

Apparatus

The flow injection manifold used is shown in Figure 6. The reagent streams were pumped by an Isco (Lincoln, NE) Tris model peristaltic pump. Samples were introduced with a Rheodyne (Cotati, CA) model 7125 sample injection valve with a 10 μ l loop. All tubing was Teflon from the Anspec Company, Inc. (Ann Arbor, MI) with 0.5 mm internal diameter. The reaction coil, 200 cm long, was thermostated by immersing it in a water bath with a Techne TE-7 circulator (Cambridge, England). For fluorescence measurement, a Varian (Palo Alto, CA) model Fluorichrom detector with a 25 μ l total volume flow cell was used. A combination of Varian filters was selected for 355 nm excitation wavelength and 435 nm emission wavelength. A Kratos (Ramsey, NJ) model Spectroflow 757 absorbance detector with a 12 μ l flow cell was set at a wavelength of 355 nm to measure the absorbance of the product. The output signals were recorded on a strip chart OmniScribe recorder, Houston Instrument (Austin, TX). The pH of the reagent solutions were measured with a Corning (Medfield, MA) model pH meter 130.

For kinetic studies, the reaction was followed spectrophotometrically by measuring the rate of change in the absorbance of

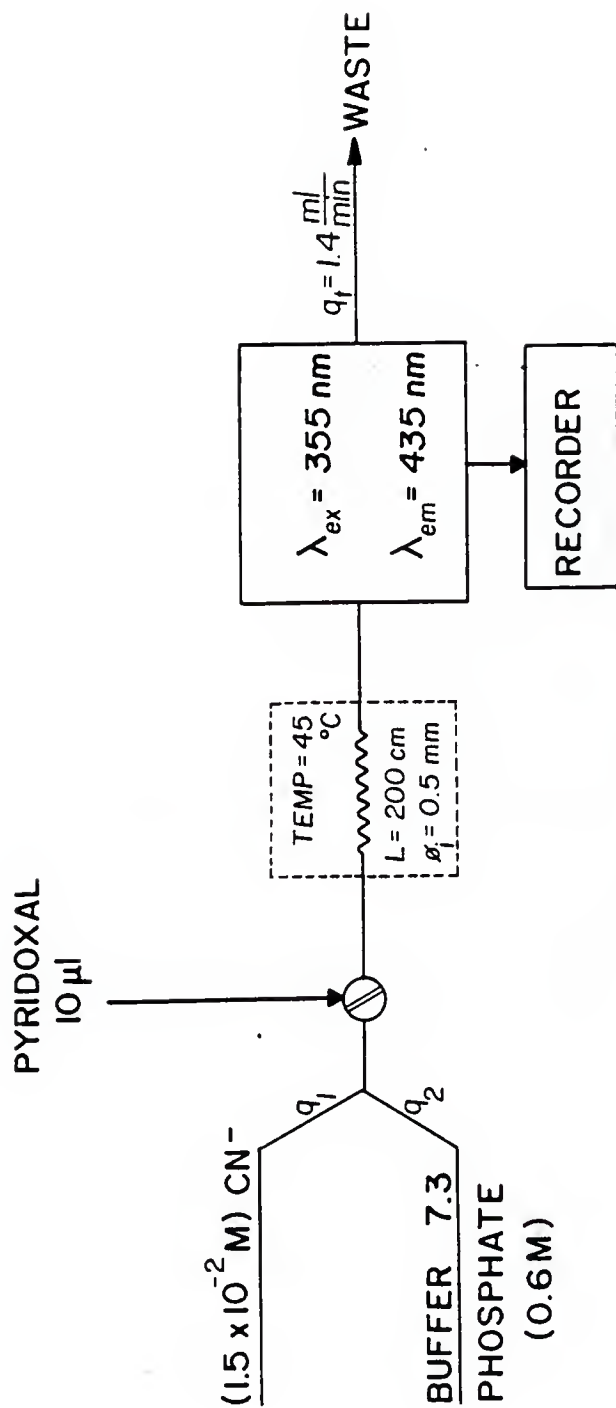


Figure 6. FIA manifold for the determination of pyridoxal.

4-pyridoxolactone, at 355 nm using a Hewlett Packard (San Diego, CA) model 8450A Diode Array spectrophotometer connected to a Hewlett Packard model 7470A plotter.

Reagents

All reagents were used as received and prepared either in deionized water or in surfactant solutions. The cationic surfactant was hexadecyltrimethylammonium bromide (CTAB, purum grade) from Fluka Chemical (Hauppauge, NY). Standard solutions of pyridoxal, Sigma grade (Sigma Chemical Company, St. Louis, MO) and solutions of potassium cyanide, certified ACS, from Fisher Scientific Company (Fair Lawn, NJ) were used for this study. Phosphate buffer solutions (0.6 M) certified ACS from Fisher Scientific Company were prepared and the pH was adjusted with concentrated hydrochloric acid, ACS certified, from Mallinckrodt (Paris, KY).

Procedure

The appropriate weight of surfactant was dissolved in distilled water and the solution then filtered through a 0.45 μ m nylon-66 membrane filter (Rainin Instruments, Woburn, MA). Appropriate amounts of pyridoxal and cyanide were dissolved either in distilled H₂O or micellar solution. All reported values are averages of at least four determinations.

CHAPTER IV
MICELLAR CATALYSIS IN THE DETERMINATION OF
PYRIDOXAL BY FLOW INJECTION ANALYSIS

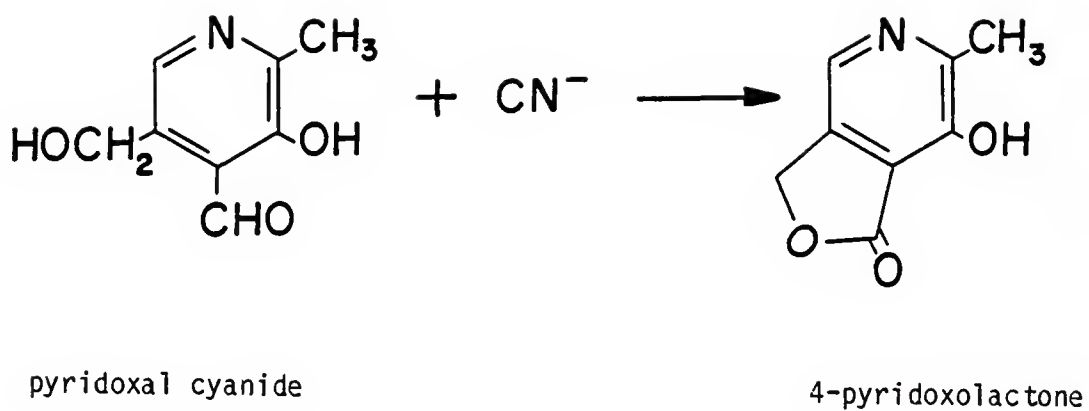
Results and Discussion

Pyridoxal is one of the three substances designated as vitamin B₆. Determination of pyridoxal and its derivatives is of great interest, especially in clinical chemistry. A fundamental role for pyridoxal has been postulated in the mechanism for active transport of amino acids and metals ions across the cell membrane (46).

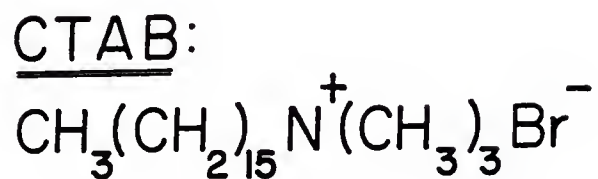
The analysis of pyridoxal in biological material has proven to be difficult and unsatisfactory. Pyridoxal has been analyzed via high pressure liquid chromatography (HPLC) with amperometric, enzymatic-fluorometric or photometric detectors and via radiochemical means. The most common detection procedure for pyridoxal is fluorimetry, involving the use of Zn-glycine or formation of hydrazone derivatives (47).

P. Linares and coworkers (47) reported a fluorimetric method for determination of pyridoxal by flow injection analysis. This method was based on the oxidation of pyridoxal in the presence of cyanide to yield 4-pyridoxolactone (see Figure 7a).

There is no spectral evidence of reaction between cyanide and the other vitamin B₆ derivatives. These results indicate that the carbonyl is the only group in the pyridoxal molecule capable of reacting with cyanide (48-50).



(a)



(b)

Figure 7. Reaction and surfactant media used for the analysis of pyridoxal. Reaction for pyridoxal with cyanide (a) and CTAB's molecular formula (b).

Preliminary studies on the behavior of this reaction are shown in Figures 8 and 9. At a wavelength interval of 280 to 400 nm, the change in absorbance versus time was recorded for aqueous and micellar media. The cationic surfactant, CTAB, was chosen to attempt to promote the rate of this reaction (see Figure 7b). A CTAB concentration of 0.05 M was used which is safely above the CMC of 0.0013 M at 25°C (30). Maximum absorbance was found to be at 355 nm for the pyridoxal-cyanide reaction product for both aqueous and micellar media. In agreement with the expected results, the cationic surfactant, CTAB, promotes the rate of the reaction. Greater changes in absorbance were absorbed in micellar media during the same amount of time. This increase in the rate of the reaction can be explained by electrostatic attraction forces between the positive charge at the micelle surface and the negative charge of the cyanide. Also, the hydrophobic forces between the pyridoxal molecule and the nonpolar portion of the micelle caused the reaction to proceed at faster rate. Not only the solubilization and proximity effects contribute (24,43) to micellar catalysis, but probably the stabilization of some intermediate species with partial negative charge at the positive micelle surface favored the formation of 4-pyridoxolactone.

Kinetics studies were performed to measure the rate constants for this oxidation reaction in aqueous and 0.05 M CTAB media. Figures 10 and 11 show the curves of the change in absorbance versus time at a maximum absorbance wavelength of 355 nm. For micellar media, the reaction reached the plateau of the curve after 15 minutes, whereas in aqueous media the plateau was reached after 30 minutes.

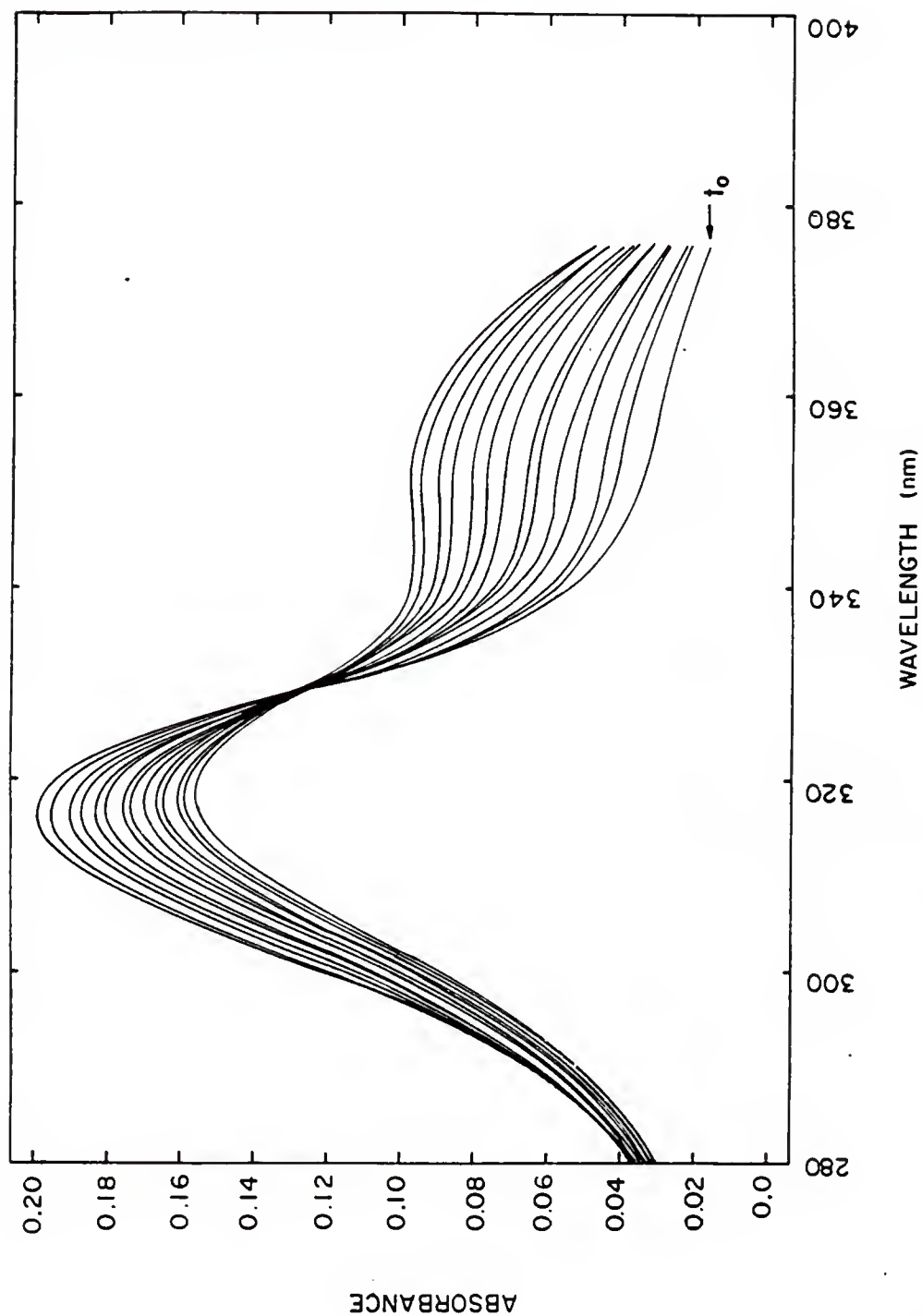


Figure 8. Absorbance versus wavelength (nm) in aqueous system for the determination of pyridoxal. Phosphate buffer (0.6 M), pH 7.3, 0.61 ppm pyridoxal, KCN 7.5×10^{-3} M, 1 cm cell, at room temperature. Spectra were run at 1 minute intervals.

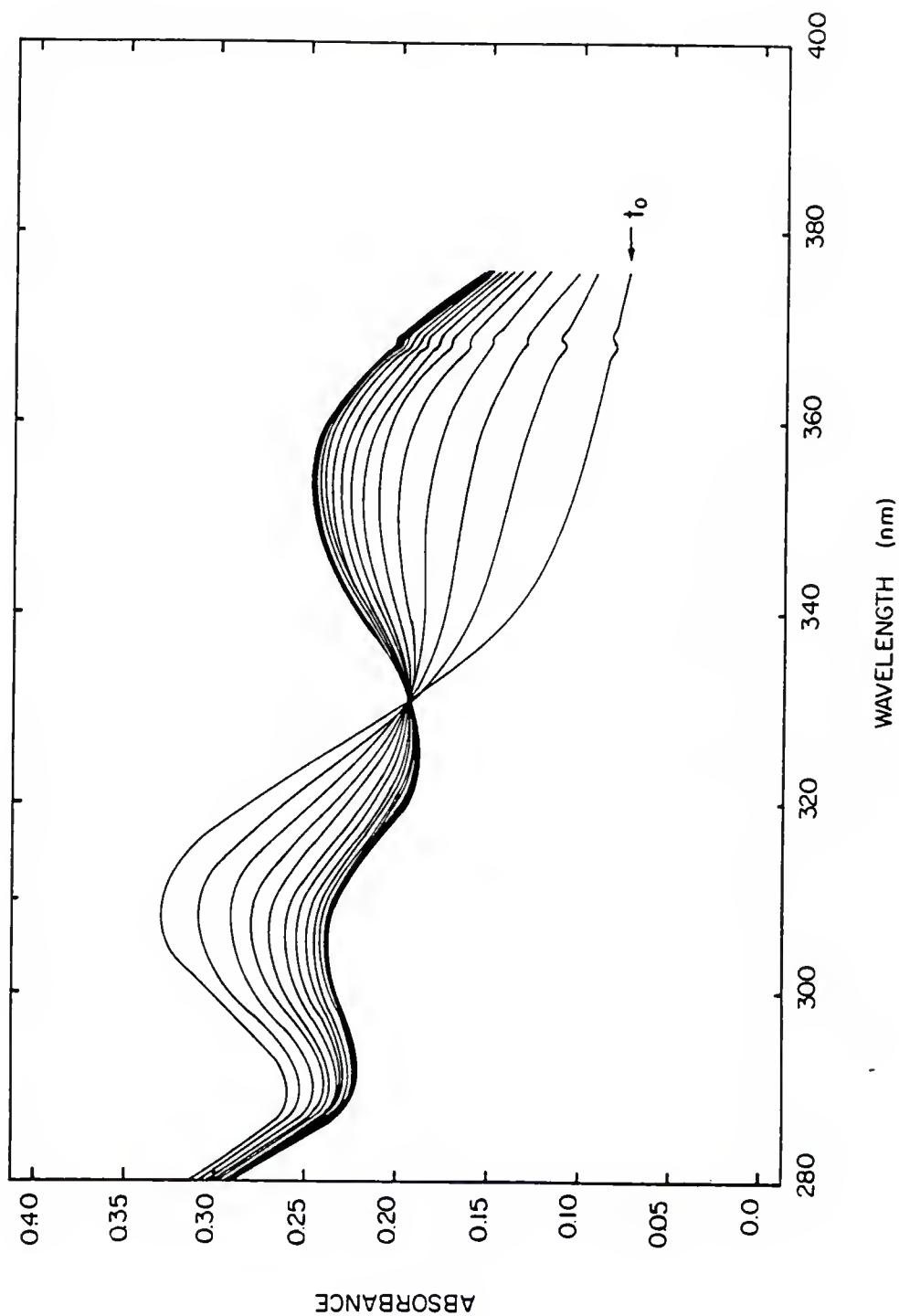


Figure 9. Absorbance versus wavelength (nm) in 0.05 M CTAB micellar system for the determination of pyridoxal. Phosphate buffer (0.6 M), pH 7.3, 0.61 ppm pyridoxal, KCN 7.5×10^{-3} M, 1 cm cell, at room temperature. Spectra were run at 1 minute intervals.

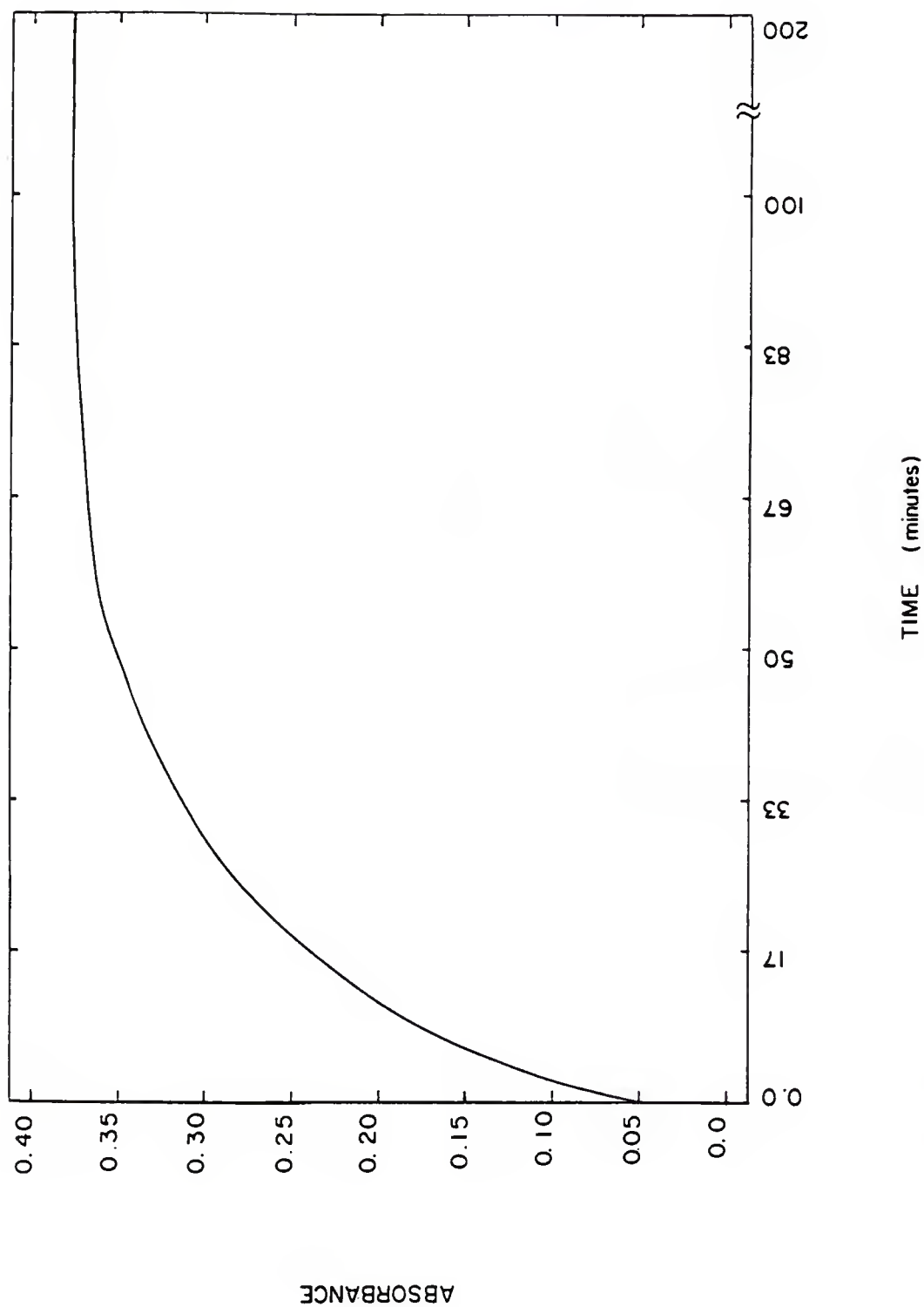


Figure 10. Change in maximum absorbance (355 nm) versus time (minutes) in aqueous media for the determination of pyridoxal. Pyridoxal 0.93 ppm, phosphate buffer 0.6 M, pH 7.3, KCN 7.5×10^{-3} M, 1 cm cell, at room temperature.

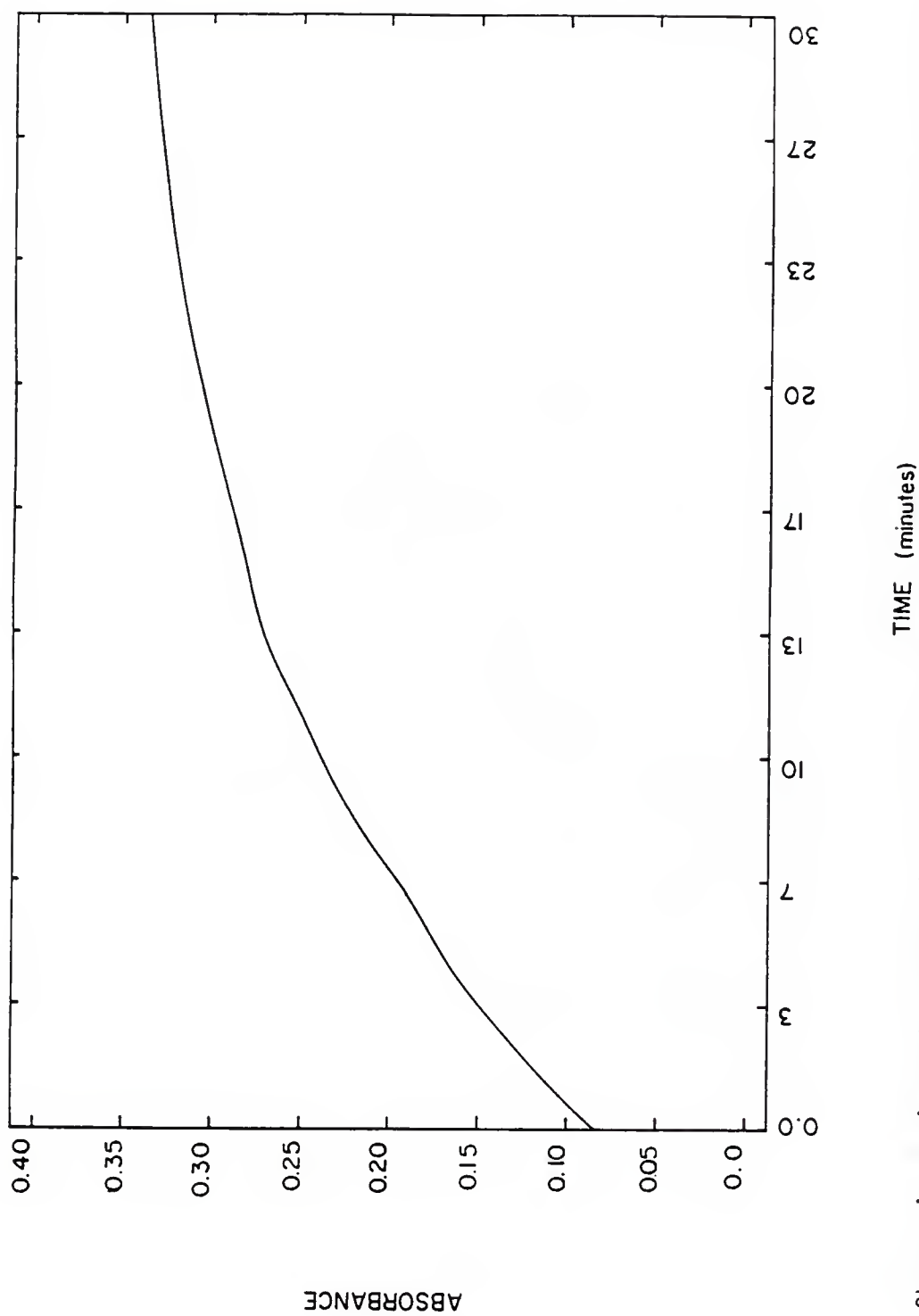


Figure 11. Change in maximum absorbance (355 nm) versus time (minutes) in 0.05 M CTAB micellar media for the determination of pyridoxal. Pyridoxal 0.93 ppm, phosphate buffer 0.6 M, pH 7.3, KCN 7.5×10^{-3} M, 1 cm cell, at room temperature.

Assuming the reaction is pseudo first order, the rate constant can be calculated by using the following equation:

$$\log (A_{\infty}-A_t) = \frac{-kt}{2.303} + \log (A_{\infty}-A_0) \quad (\text{eq. 4.1})$$

where A_{∞} , A_0 , A_t are the absorbance at infinite, initial and time t , respectively; t is time in minutes; and k is the rate constant in minutes⁻¹ (51). From the slope of the curve (taking the negative and multiplied by 2.303) the rate constants for the reaction of pyridoxal taking place in water and 0.05 M CTAB media were 0.0490 and 0.0971 minutes⁻¹ (see Figures 12 and 13). The ratio of these rate constants, $k_{0.05\text{M CTAB}}/k_{\text{H}_2\text{O}}$, is equal to 1.98. This value means that the reaction is taking place at double the velocity in micellar CTAB than in H_2O . Micellar catalysis does occur for this particular reaction.

To demonstrate the advantages of combining the technique of FIA with micellar catalysis, measurements of the pyridoxal-cyanide reaction product using absorbance and fluorescence detection were carried out. Figure 14 shows the calibration plot for the pyridoxal determination in aqueous and 0.05 M CTAB media. Comparing the slope of both curves, 2.54×10^{-3} and 3.26×10^{-3} absorbance units/ppm of pyridoxal, one can observe that by using a CTAB micellar media the sensitivity of the system is increased 1.3 times. The differences between the ratio of rate constants found for water and 0.05 M CTAB, 1.98, and the ratio of sensitivities of these two systems by FIA, 1.3, may be explained by the fact that the kinetics throughout the entire sample plug is not constant. The work of Paiton and Mottola (37)

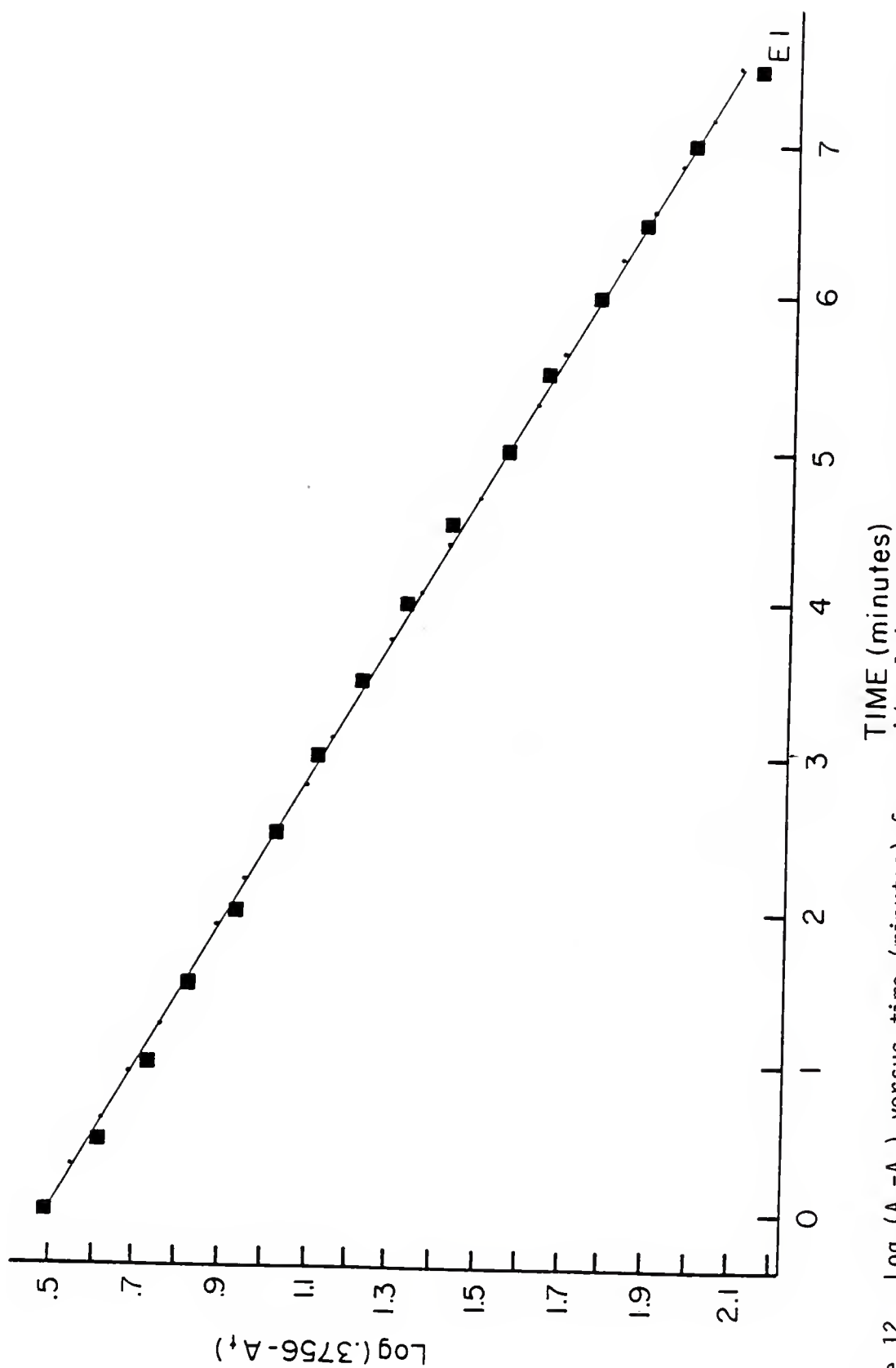


Figure 12. $\text{Log}(A_\infty - A_t)$ versus time (minutes) for pyridoxal in aqueous system. Absorbance measured at 355 nm, pyridoxal 0.93 ppm , in 1 cm cell at room temperature, phosphate buffer (0.6 M) , pH 7.3, $\text{KCN } 7.5 \times 10^{-3} \text{ M}$.

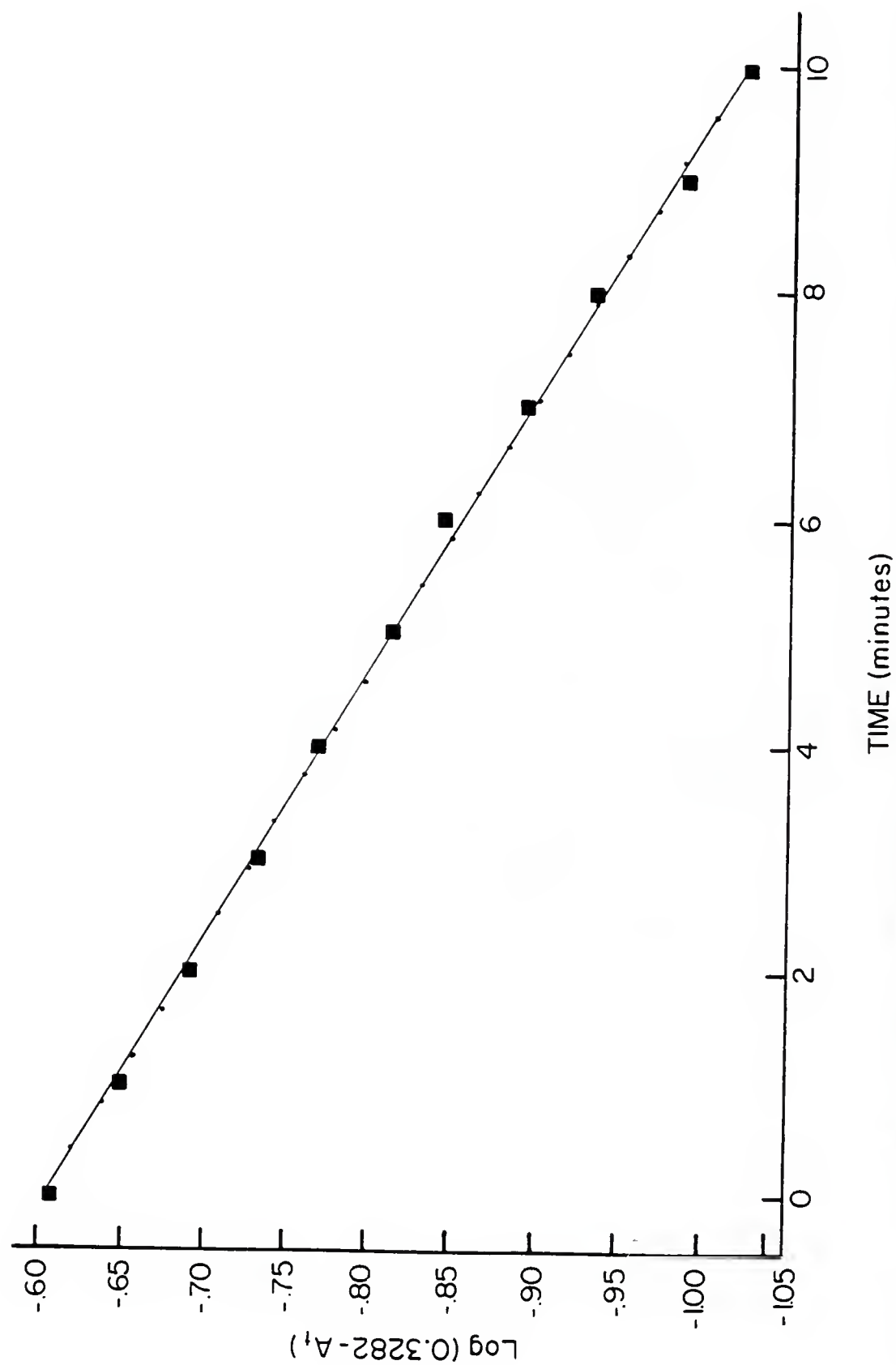


Figure 13. $\text{Log}(A_\infty - A_t)$ versus time (minutes) for pyridoxal in 0.05 M CTAB system. Absorbance measured at 355 nm, pyridoxal 0.93 ppm, in 1 cm cell at room temperature, phosphate buffer (0.6 M), pH 7.3, KCN 7.5×10^{-3} M.

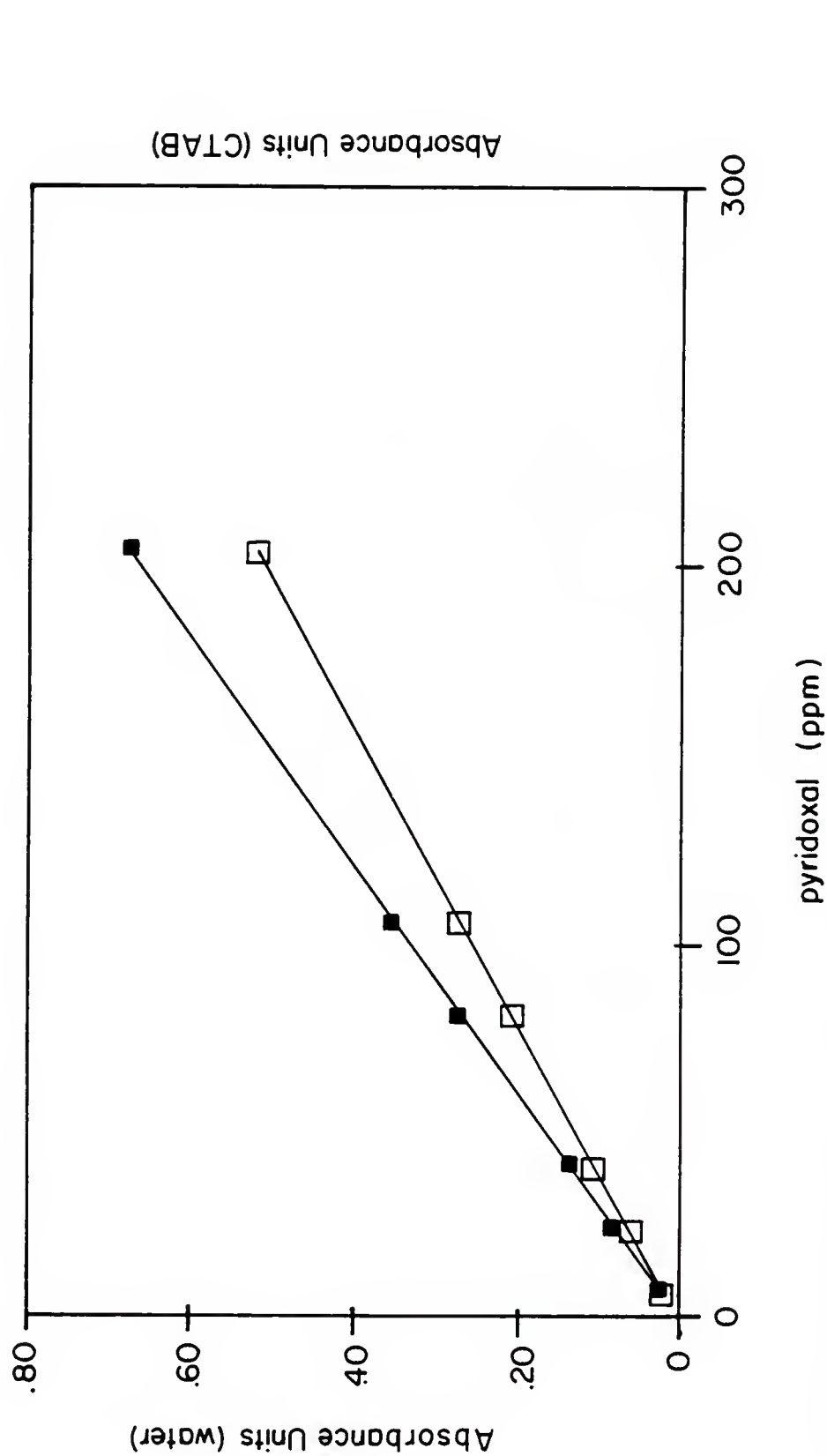


Figure 14. Absorbance calibration plots for pyridoxal in aqueous (□) and 0.05 M CTAB (■) systems. Absorbance measured at 355 nm, flow rate 1.4 ml/min, temperature 45°C, pH 7.3, phosphate buffer (0.6 M), KCN 1.5×10^{-2} M.

demonstrated that the assumption of having a constant rate coefficient throughout the entire body of the sample plug is invalid. The kinetics involved within the sample plug are more complex. Paiton and Mottola suggested that the rate coefficient changes with time. This has been rationalized by assuming that each fluctuation in rate coefficient with time corresponds with one of three regions within a sample plug, namely, the leading region, the central region, and the trailing region. In both the leading and trailing regions, the carrier/sample interfaces induce molecular diffusion, while the velocity profile induces convection. In the central region, where no sample/carrier boundary exists, convection becomes the primary dispersion force. Because the physical dispersion in these three regions of the sample plug differ from one another, the rate coefficients along the length of the plug are expected to vary with a wave pattern. The fact that the reaction rate varies throughout the sample plug may mean also that the kinetic order is not constant within the sample plug.

Figure 15 shows the calibration plot with a fluorescence detector for aqueous and micellar systems. From the slope of the curves, the calculated sensitivity of the pyridoxal system is three times greater when using CTAB micellar media compared with the same system in aqueous media. The sensitivities for micellar and aqueous solutions were 0.294 and 0.102 cm (peak height) per ppm of pyridoxal, respectively. A greater change in the ratio of sensitivities was observed for fluorescence determination due to the fact that not only micellar catalysis was taking place but fluorescence enhancement was

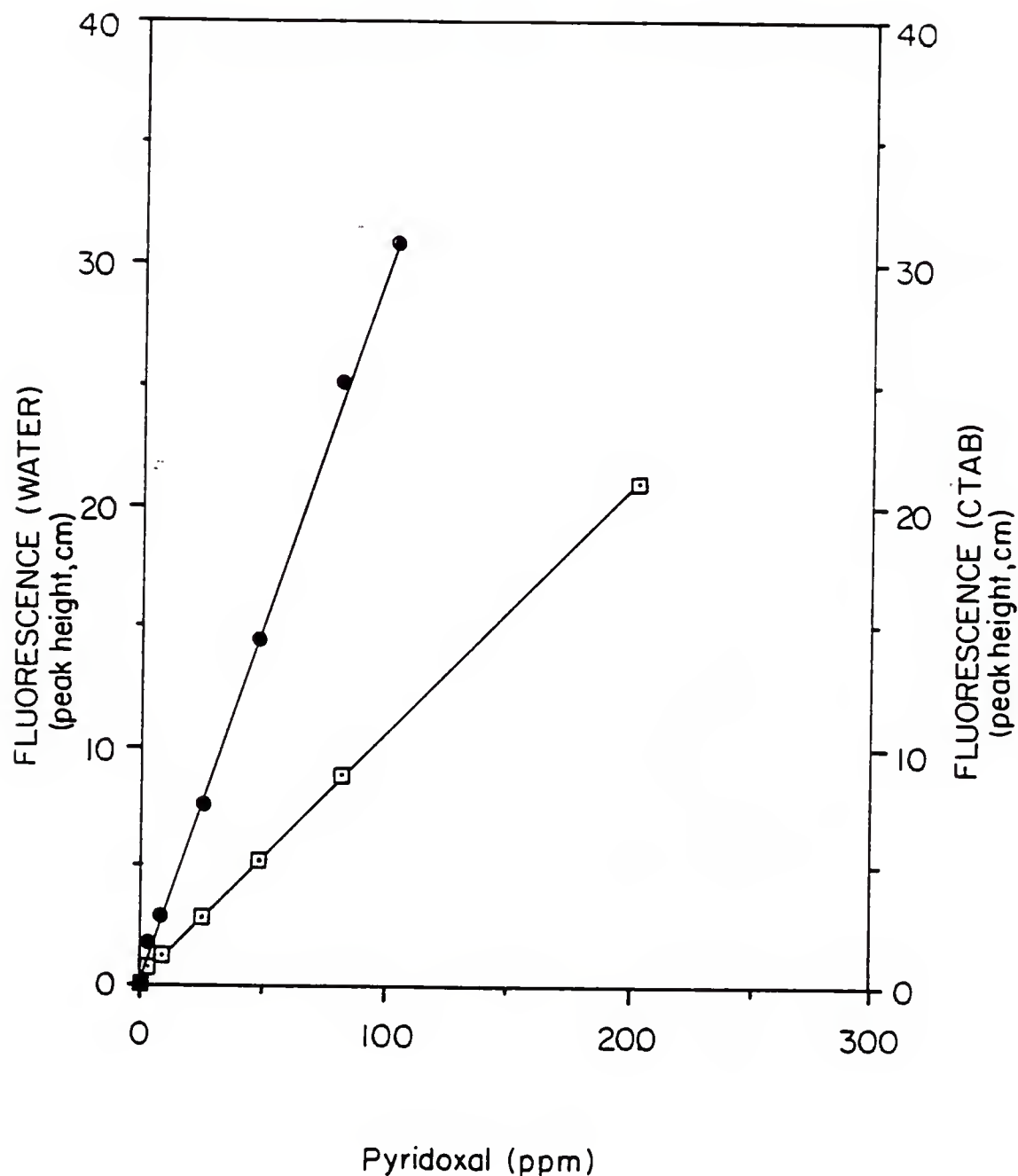


Figure 15. Fluorescence calibration plots for pyridoxal determination in aqueous (□) and 0.05 M CTAB (●) systems. Flow rate 1.4 ml/min; temperature 45°C; phosphate buffer (0.6 M); pH 7.3; KCN 1.5×10^{-2} M; 355 and 435 nm excitation and emission wavelengths, respectively.

also observed. In micellar-enhanced fluorescence, the emission intensity of the analyte is usually many times greater than in the corresponding homogeneous media (52,53). This increase in sensitivity of solutes in solutions containing micellar aggregates has been explained by the diminution of deactivation processes for the excited states. These phenomena occur due to a decrease in polarity, and an increase in viscosity and shielding against quenching in micellar media (29).

Table I summarizes the analytical figures of merit for both aqueous and micellar systems. Very good coefficients of correlation were obtained for the four curves, all being 0.999. These calibration curves recorded under working conditions are linear over a wide range of concentrations. The linear range for the aqueous system with a fluorescence detector was found to be from 0.42 ng to 2.0×10^3 ng and from 94 ng to 2.0×10^3 ng of pyridoxal for absorbance measurement. For 0.05 M CTAB media the linear dynamic range was from 0.17 ng to 1.1×10^3 ng of pyridoxal for fluorescence and from 77 ng to 2.0×10^3 ng of pyridoxal for absorbance. Due to the large concentration range for the recorded curves, it was necessary to work at several values of the instrument sensitivity. At higher concentrations of pyridoxal, the fluorescence intensity is beyond the spectrofluorimeter range. The reproducibility of the system was measured by manual injection of 11 replicates of pyridoxal solution at 25.53 ppm. Relative standard deviation of peak height in percent was calculated and was found to vary between 0.97 and 3.25 for the studied systems. Limits of detection were found to be lower for the reaction taking place in

Table I. Figures of merit for pyridoxal determination. Fluorescence detector: excitation 355 nm, emission 435 nm, range 500, or variable UV-visible absorbance detector at 355 nm, range .1, 1.5×10^{-2} M cyanide, pH 7.3, phosphate buffer 0.6 M, flow rate 1.4 ml/min, temperature 30°C, chart speed 1 cm/min, 10 μ l sample loop, pyridoxal in deionized water, tube length 200 cm, i.d. 0.5 mm.

	Fluorescence		Absorbance	
	Aqueous	0.05 M CTAB	Aqueous	0.05 M CTAB
Sensitivity ^a	0.102	0.294	2.54×10^{-3}	3.26×10^{-3}
Coefficient of correlation	0.9996	0.9992	0.9999	0.9999
Limits of detection (ng)	0.42	0.17	94	77
Relative standard deviation (%) ^b	2.06	3.25	0.97	1.76

^a Slope of the calibration plot for fluorescence, cm/ppm of pyridoxal and absorbance units/ppm of pyridoxal for absorbance measurements.

^b Eleven determinations at 25.53 ppm of pyridoxal.

micellar solutions. A more significant change in limits of detection was not obtained due to an increase in the background signal for micellar solutions. This needs further study in the future the examination of other systems in micellar media by FIA, since a significant change in limits of detection usually accompanies micellar catalysis (52).

Optimum conditions may be different for aqueous and micellar systems. The reason for this difference is that micelles can change the microenvironment of the solubilized molecules (22). Then, an optimization of conditions for FIA system is required.

The output signal, in this case peak height, is influenced by the dispersion of the sample in the reagent stream and the degree of completeness of the reaction taking place. These two are affected by experimental parameters such as flow rate, reagent concentrations, length of the reaction coil, etc. Since these experimental parameters interact with each other, optimization of FIA methods using univariate design (optimization of every parameter by separate studies) is time consuming and may be inadequate to determine the best set of experimental conditions (54). Sequential simplex optimization procedures have been found to be valuable in development of new FIA methods (54-56).

A modified variable size simplex method (57,58) was used for optimization of pyridoxal determination. The optimization of this system was performed by changing four variables: pH, temperature, flow rate and surfactant concentration. Table II shows the initial, final and increment values for each changing parameter. The reason to

Table II. Variable parameters for the Modified Simplex Optimization program.

Parameter	Initial Value	Range Value	Increment Value
1. pH	7.3	6.5-8.0	0.5
2. Flow rate (ml/min)	1.4	1.0-1.7	0.1
3. Temperature (°C)	45	30-50	5
4. CTAB concentration (M)	0.05	0.05-0.15	0.05

include pH as one of the parameters to be optimized is that the reaction of pyridoxal with cyanide is pH dependent. It is reported in the literature that micelles affect the pH of solutions, by changing acid dissociation constants (59). The range of pH from 6.5 to 8.0 was chosen because previous studies showed this to be the optimal pH range for the oxidation reaction. An increase in temperature increased the reaction rate in such a manner that higher values for the response function resulted, up to a certain point where the signal started to decrease as the temperature increased due to deactivation of fluorescence. At temperatures below 30°C, the response of the system (peak height) is greatly diminished; at temperatures above 50°C, bubble formation in the FIA system can prove detrimental to reproducibility (47). Flow rate is closely related with the output signal (vide supra). Faster flow rates will usually lead to a decrease in signal because less time is available for the reaction to take place and vice versa. The surfactant concentration was included as a variable since increasing the number of micellar structures increases the number of sites available for solute solubilization and, therefore, promotes the formation of 4-pyridoxolactone. If the surfactant concentration is increased too much, the reaction will occur at a lower rate due to the dilution factor. In other words, as the number of micelle structures increases, solute molecules will be solubilized on different micelle structures apart from each other. There will be a physical impediment for a pyridoxal molecule to encounter a cyanide ion preventing the oxidation reaction to proceed. The cyanide concentration and the length of reaction coil

were kept constant. At a cyanide concentration of fivefold the pyridoxal concentration, the intensity of the output signal is not influenced by a change in the cyanide concentration (47). The simplex was finished after 18 experiments (one reflection, two expansions and four contractions). Optimum values found, together with those variables kept constant throughout the development of the simplex, are summarized in Table III.

With these new optimum values for absorbance measurement in CTAB media, a set of standard pyridoxal solutions were run and a calibration plot was recorded and compared with the calibration plot for the water system run with previous conditions (see Figure 16). A ratio of 1.8 was found, by comparing the slopes of the two curves, for water and CTAB, 2.09×10^{-3} and 3.84×10^{-3} absorbance units per parts per million of pyridoxal. As was expected, a higher sensitivity was observed. This can be explained by the fact that now the conditions are more favorable for the reaction to take place. Table IV shows the analytical figures of merit for the reaction in optimized CTAB conditions and previous conditions for aqueous system. Relative standard deviation, measured by 11 determinations of 24.14 ppm of pyridoxal, were 1.06 and 2.12% for CTAB and water systems. Very good coefficients of correlation were observed for both curves, 0.999, assuring the linearity of the curve. Lower limits of detection were obtained by using 0.09 M CTAB and 49°C, 64 ng, compared with the aqueous system, 86 ng.

Figures 17 to 21 show a set of pyridoxal standard solutions run by FIA under different studied conditions.

Table III. Optimized and fixed variables for the determination of pyridoxal.

Variables Fixed in the Optimization	Optimized Variables
1. 10 μ l sample: Pyridoxal: 9.18 $\times 10^{-4}$ M in 0.05 M CTAB	1. pH: 6.74
2. Cyanide concentration: 1.5 $\times 10^{-2}$ M	2. Flow rate: 1.3 ml/min
3. Phosphate buffer solution: 0.6 M	3. Temperature: 49°C
4. Length of reaction coil: 200 cm	4. CTAB concentration: 0.09 M

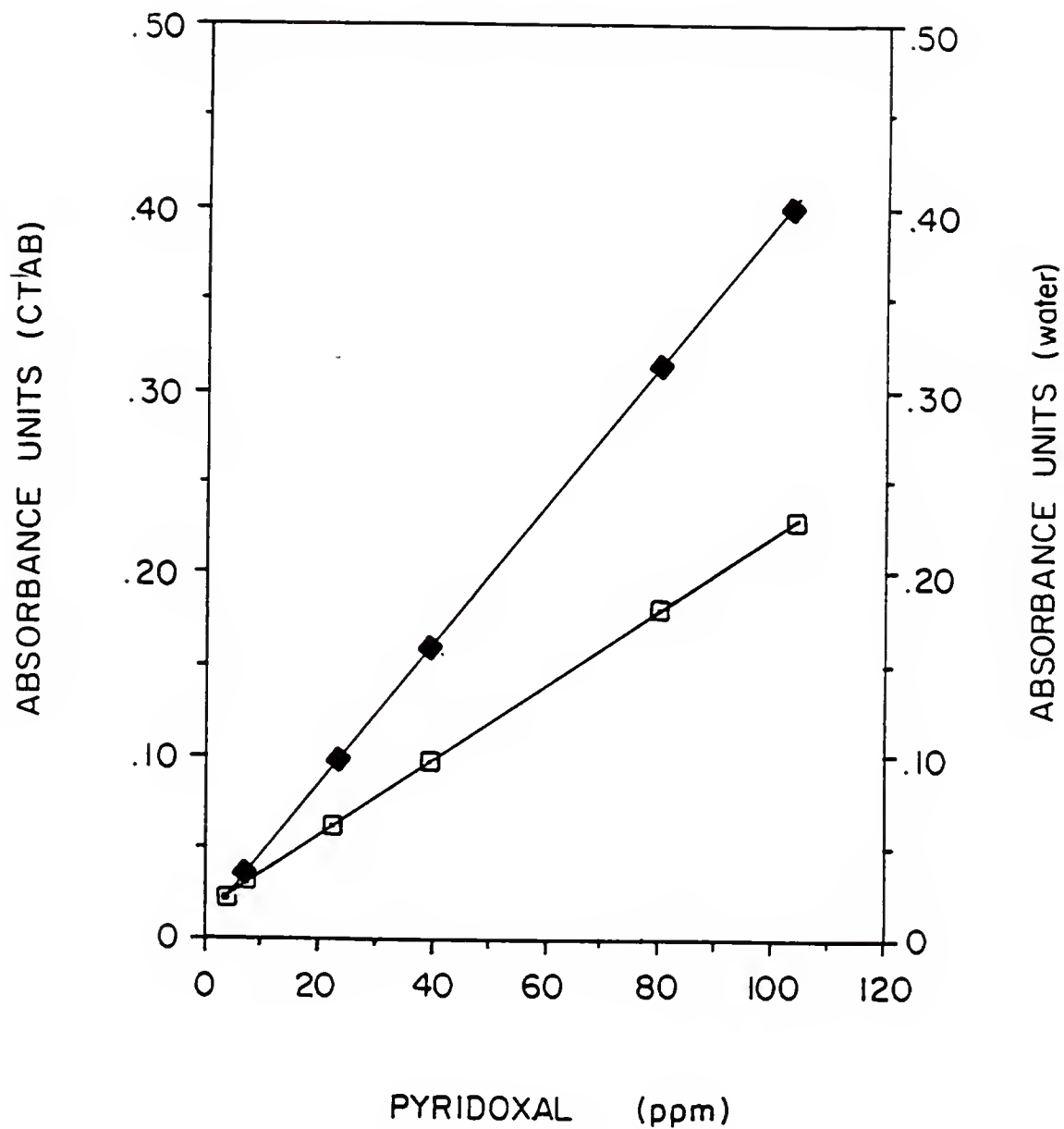


Figure 16. Absorbance calibration plots for pyridoxal in aqueous (□) and 0.09 M CTAB micellar (■) media. Absorbance measured at 355 nm, flow rate 1.3 ml/min, temperature 49°C, pH 6.74, phosphate buffer (0.6 M), KCN 1.5×10^{-2} M.

Table IV. Figures of merit for pyridoxal determination with conditions obtained by Modified Simplex program. Variable UV-visible absorbance detector at 355 nm, range .1, 0.09 M CTAB, 1.5×10^{-2} M cyanide, pH 6.74, 0.6 M phosphate buffer, flow rate 1.3 ml/min, temperature 49°C, chart speed 1 cm/min, 10 μ l sample loop, pyridoxal in deionized water, tube length 200 cm, i.d. 0.5 mm.

	Aqueous	CTAB
Sensitivity ($\frac{\text{absorbance units}}{\text{ppm of pyridoxal}}$)	2.09×10^{-3}	3.84×10^{-3}
Coefficient of correlation	0.9994	0.9998
Limits of detection (ng)	86	64
Relative standard deviation (%) ^a	2.12	1.06

^a Eleven determinations at 24.14 ppm of pyridoxal.

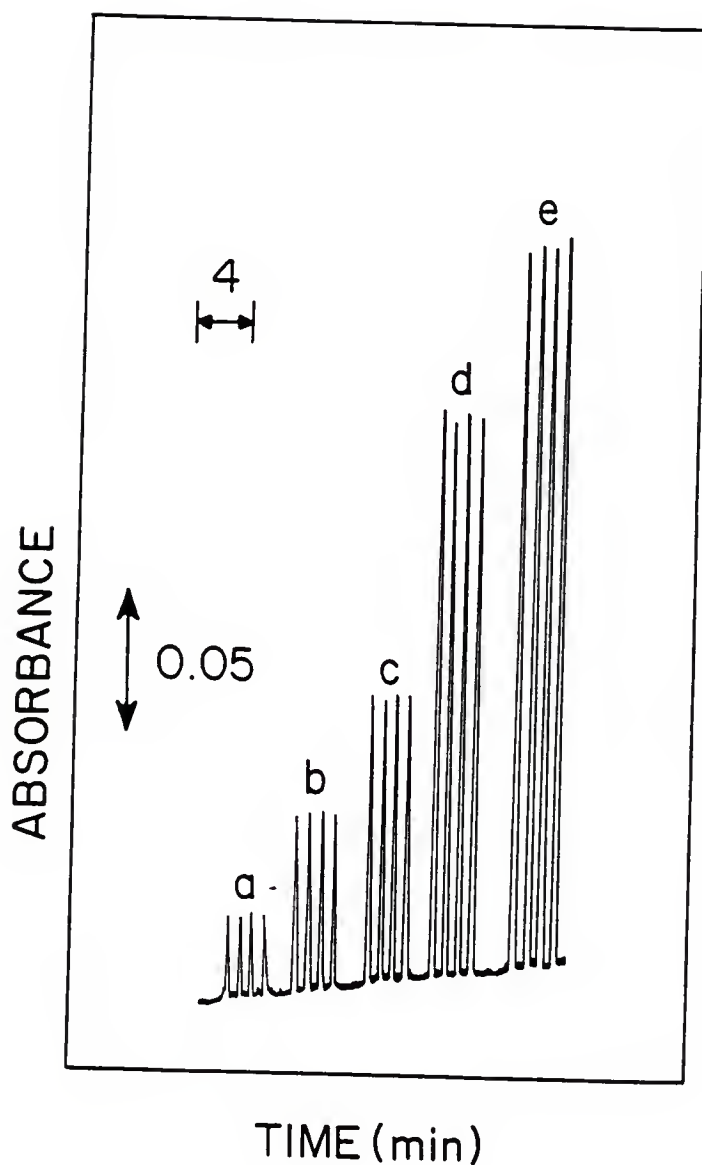


Figure 17. Absorbance recordings of a series of pyridoxal standards in aqueous media. Pyridoxal: (a) 8.10 ppm, (b) 24.31 ppm, (c) 40.52 ppm, (d) 81.04 ppm, (e) 105.4 ppm. Absorbance measured at 355 nm, range 0.05, sample volume 10 μ l, all tubes 0.5 mm I.D., flow rate 1.4 ml/min, temperature 45°C, phosphate buffer 0.6 M, pH 7.3, KCN 1.5×10^{-2} M, chart speed 0.25 cm/min.

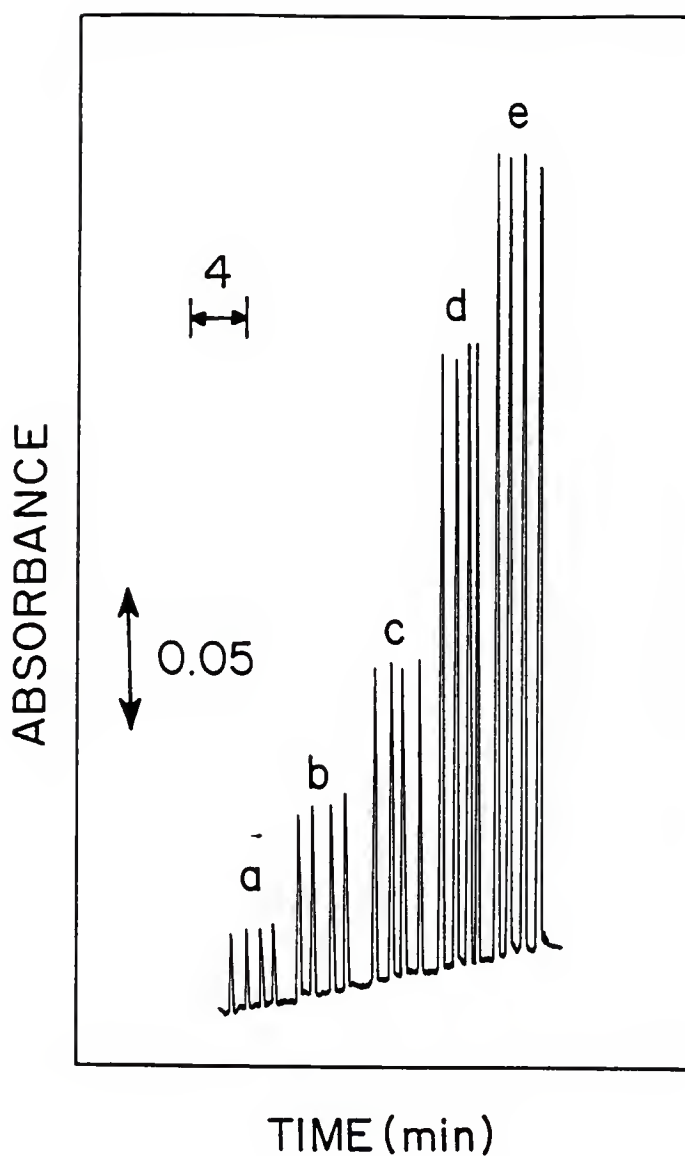
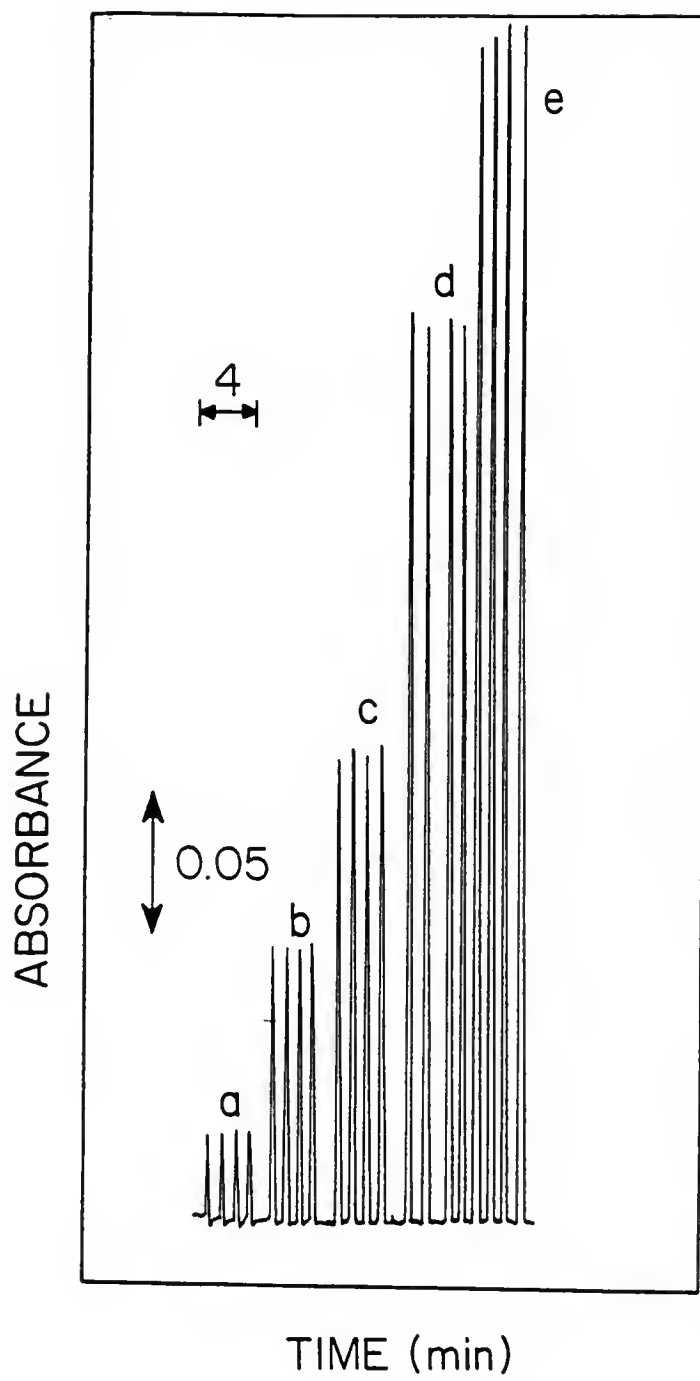


Figure 18. Absorbance recordings of a series of pyridoxal standards in 0.05 M CTAB micellar media. Pyridoxal: (a) 8.10 ppm, (b) 24.31 ppm, (c) 40.52 ppm, (d) 81.04 ppm, (e) 105.4 ppm. Absorbance measured at 355 nm, range 0.05, sample volume 10 μ l, all tubes 0.5 mm I.D., flow rate 1.4 ml/min, temperature 45°C, phosphate buffer 0.6 M, pH 7.3, KCN 1.5×10^{-2} M, chart speed 0.25 cm/min.

Figure 19. Absorbance recordings of a series of pyridoxal standards in 0.09 M CTAB micellar media. Pyridoxal: (a) 8.10 ppm, (b) 24.31 ppm, (c) 40.52 ppm, (d) 81.04 ppm, (e) 105.4 ppm. Absorbance measured at 355 nm, range 0.05, sample volume 10 μ l, all tubes 0.5 mm I.D., flow rate 1.3 ml/min, temperature 49°C, phosphate buffer 0.6 M, pH 6.73, KCN 1.5×10^{-2} M, chart speed 0.25 cm/min.



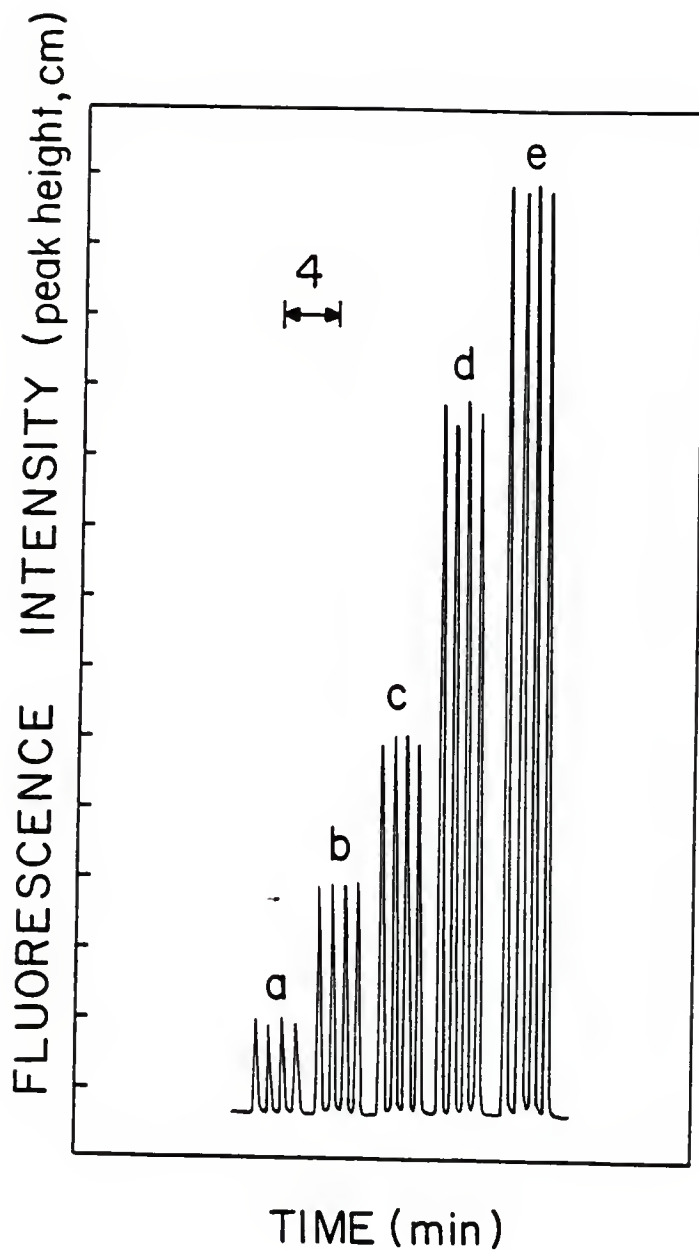
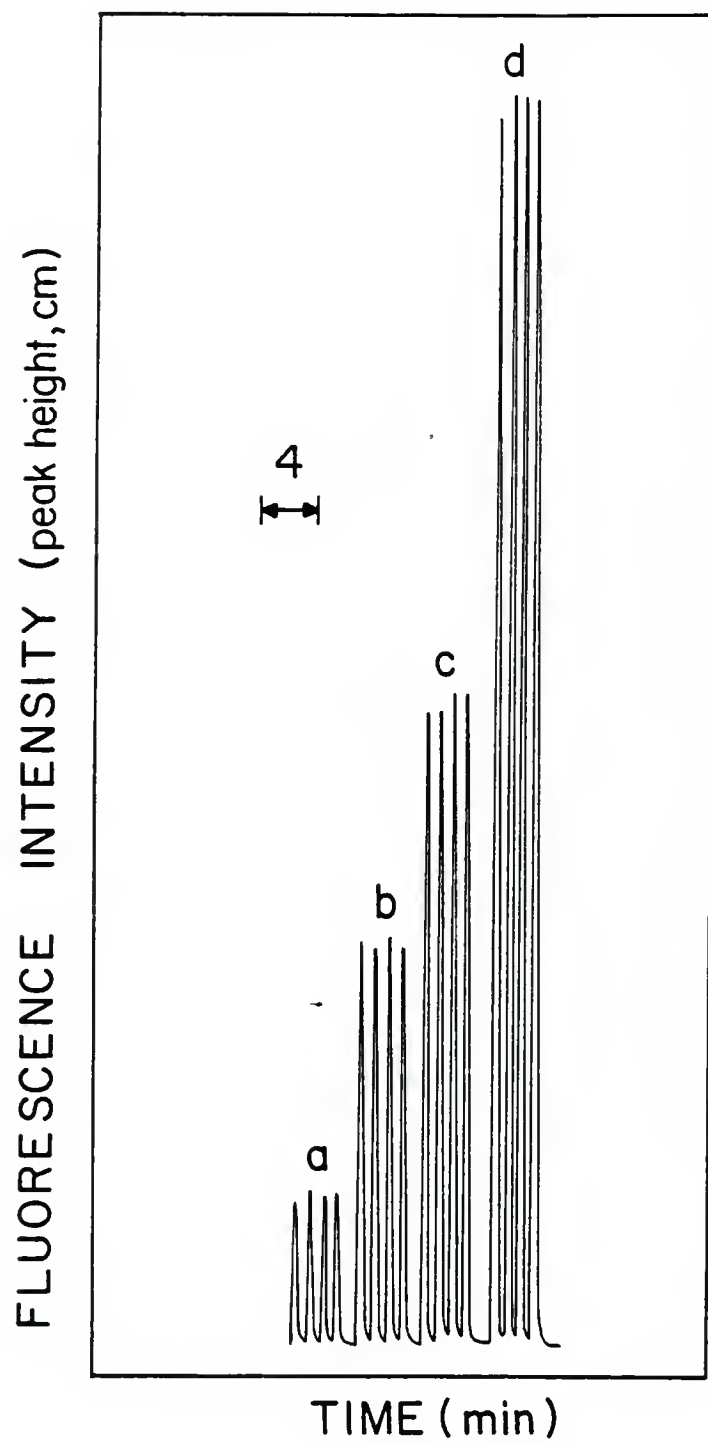


Figure 20. Fluorescence recordings of a series of pyridoxal standards in aqueous media. Pyridoxal: (a) 8.10 ppm, (b) 24.31 ppm, (c) 40.52 ppm, (d) 81.04 ppm, (e) 105.4 ppm. Sample volume 10 μ l; all tubes 0.5 mm I.D.; flow rate 1.4 ml/min; temperature 45°C; phosphate buffer 0.6 M; pH 7.4; KCN 1.5×10^{-2} M; range 1000; chart speed 0.25 cm/min; 355 nm and 435 nm excitation and emission wavelengths, respectively.

Figure 21. Fluorescence recordings of a series of pyridoxal standards in 0.05 M CTAB micellar media. Pyridoxal: (a) 8.10 ppm, (b) 24.31 ppm, (c) 40.52 ppm, (d) 81.04 ppm. Sample volume 10 μ l; all tubes 0.5 mm I.D.; flow rate 1.4 ml/min; temperature 45°C; phosphate buffer 0.6 M; pH 7.4; KCN 1.5×10^{-2} M; 355 nm and 435 nm excitation and emission wavelengths, respectively; range 1000; chart speed 0.25 cm/min.



Measurements of Dispersion

In flow injection analysis, both sample throughput and sample dilution are directly related to dispersion. The dispersion process which takes place during the transport of the sample from the injection device toward the detector is one of the less understood aspects of FIA (*vide supra*). In analogy with chromatographic systems, Poppe (60) observed that the total peak broadening in FIA is the sum of the contributions from the injection process, the flow through reactors and connectors, the holdup volume of the flow through detector, and the time constants of associated electronics. These processes can be described by the individual peak variances:

$$\sigma_{\text{overall}}^2 = \sigma_{\text{injection}}^2 + \sigma_{\text{flow}}^2 + \sigma_{\text{detector}}^2$$

Provided that the detector and electronics are well designed, the variance of detection may be neglected (if it is at least five times smaller than the standard deviations due to injection and transport). One of the models frequently used to describe the dispersion process is the tank in series model. According to this model, the flow reactor can be considered as a series of N ideal mixers. If the number of mixing stages, N , is sufficiently high, the resulting curve has a Gaussian shape. However, in FIA, peaks mostly show a tailing character (1,42). In 1981, Reijn and coworkers (33) described the distribution curve of an FIA to be a modified Gaussian function. Note that only the physical aspects of dispersion are taken into consideration. It was assumed that there is no contribution to

dispersion due to chemical reaction between the sample and reagent stream. This assumption, however, is known to be invalid (38,42).

For our system, the FIA peaks were examined for their resemblance to Gaussian, exponentially modified Gaussian and other peak shapes by measurement of the variance, \bar{M}_2 , and the standard deviation of the parent Gaussian function, σ_G . Foley and Dorsey (61) demonstrated that the type of peak shape can be assigned by the agreement of the values \bar{M}_2 and σ_G determined from the asymmetry factor, B/A , and peak width, W , at 10, 30, and 50% peak height (see Figure 22). Equations 4.2 to 4.7 were used to calculate \bar{M}_2 and σ_G at different peak heights.

$$\bar{M}_2 = \frac{W_{0.1}^2}{1.764(B/A)_{0.1}^2 - 11.15(B/A)_{0.1} + 28} \quad (\text{eq. 4.2})$$

$$\bar{M}_2 = \frac{W_{0.3}^2}{-3.85(B/A)_{0.3}^3 + 23(B/A)_{0.3}^2 - 47.9(B/A)_{0.3} + 38.7} \quad (\text{eq. 4.3})$$

$$\bar{M}_2 = \frac{W_{0.5}^2}{-8.28(B/A)_{0.5}^3 + 41.8(B/A)_{0.5}^2 - 72.3(B/A)_{0.5} + 44.6} \quad (\text{eq. 4.4})$$

$$\sigma_G = \frac{W_{0.1}}{3.27(B/A)_{0.1} + 1.2} \quad (\text{eq. 4.5})$$

$$\sigma_G = \frac{W_{0.3}}{2.8(B/A)_{0.3} + 0.48} \quad (\text{eq. 4.6})$$

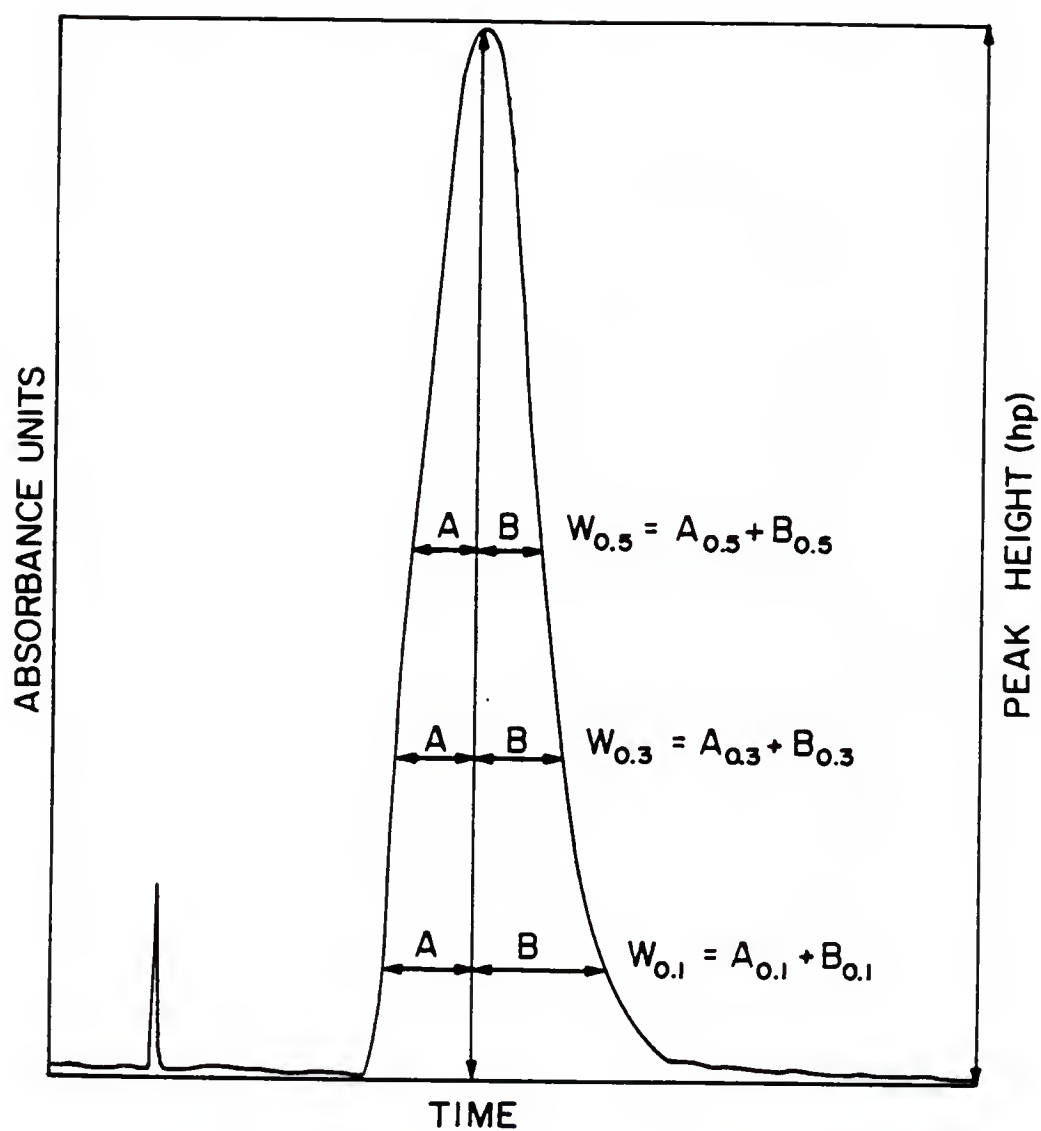


Figure 22. Measurement of peak width, W , and asymmetry factor, B/A , at 10, 30 and 50% peak height in an FIA peak.

and

$$\sigma_G = \frac{w_{0.5}}{2.5(B/A)_{0.5}} \quad (\text{eq. 4.7})$$

Tables V to X show the calculated values for the variance and standard deviation for pyridoxal in aqueous and micellar media at different peak heights. For this study, the variable wavelength absorbance detector was set at 292.6 nm, the maximum absorbance wavelength for pyridoxal. Triplicate injections of 10 μ l of pyridoxal, 2.81×10^{-4} M in aqueous solution, were made into the aqueous stream and peaks were recorded. Manual measurement of peak height, h , peak width and asymmetry factor at 10, 30 and 50% peak height were done for each peak and substitution of these values into equations 4.2 to 4.7 gave \bar{M}_2 and σ_G . Averages of three values were calculated for \bar{M}_2 and σ_G at each peak height. The same procedure was followed for 2.83×10^{-4} M pyridoxal in 0.05 M CTAB injected into 0.05 M CTAB stream. Table XI shows the average values for \bar{M}_2 and σ_G at 10, 30 and 50% peak height. The relative standard deviation of the values from the three peak heights was calculated for pyridoxal in the aqueous system to be $\pm 6.06\%$ for \bar{M}_2 and $\pm 4.88\%$ for σ_G . For 0.05 M CTAB the relative standard deviation was $\pm 5.68\%$ for \bar{M}_2 and $\pm 5.20\%$ for σ_G . According to the agreement of the values calculated at the three heights, these peaks can be classified as exponentially modified Gaussians. Foley and Dorsey (61) reported a relative standard deviation of $\pm 7.7\%$ for \bar{M}_2 or $\pm 3.2\%$ for σ_G values calculated at the three heights was necessary to ensure the validity of the

Table V. Variance and standard deviation values for pyridoxal in aqueous media at 10% peak height. Variable UV-visible absorbance detector at 292.6 nm, range .1, temperature 45°C, flow rate 1.4 ml/min, tube length 200 cm, i.d. 0.5 mm, 10 μ l sample loop, pyridoxal 2.81×10^{-4} M, chart speed 10 cm/min.

h (Peak height in cm)	14.15	14.35	14.15
$W_{0.1}$ (Width at 10% peak height in cm)	2.70	2.70	2.70
A	1.09	1.10	1.08
B	1.61	1.60	1.62
B/A (Asymmetry ratio)	1.48	1.45	1.50
\overline{M}_2 (Variance in cm^2) ^a	0.47	0.47	0.48
$\overline{X} = 0.473 \text{ cm}^2$			
$\text{RSD}^b = 1.48\%$			
σ_G (Standard deviation in cm^2)	0.447	0.454	0.442
$\overline{X} = 0.448 \text{ cm}^2$			
$\text{RSD} = 1.35\%$			

^a $1 \text{ cm}^2 = 36 \text{ s}^2$.

^b Relative standard deviation.

Table VI. Variance and standard deviation values for pyridoxal in aqueous media at 30% peak height. Variable UV-visible absorbance detector at 292.6 nm, range .1, temperature 45°C, flow rate 1.4 ml/min, tube length 200 cm, i.d. 0.5 mm, 10 μ l sample loop, pyridoxal 2.81×10^{-4} M, chart speed 10 cm/min.

h (Peak height in cm)	14.15	14.35	14.15
$W_{0.3}$ (Width at 30% peak height in cm)	1.90	2.00	1.90
A	0.80	0.85	0.80
B	1.10	1.15	1.10
B/A (Asymmetry ratio)	1.38	1.35	1.38
\overline{M}_2 (Variance in cm^2) ^a	0.57	0.55	0.57

$$\overline{X} = 0.563 \text{ cm}^2$$

$$\text{RSD}^b = 2.05\%$$

σ_G (Standard deviation in cm^2)	0.437	0.469	0.437
---	-------	-------	-------

$$\overline{X} = 0.448 \text{ cm}^2$$

$$\text{RSD} = 4.12\%$$

^a 1 $\text{cm}^2 = 36 \text{ s}^2$.

^b Relative standard deviation.

Table VII. Variance and standard deviation values for pyridoxal in aqueous media at 50% peak height. Variable UV-visible absorbance detector at 292.6 nm, range .1, temperature 45°C, flow rate 1.4 ml/min, tube length 200 cm, i.d. 0.5 mm, 10 μ l sample loop, pyridoxal 2.81×10^{-4} M, chart speed 10 cm/min.

h (Peak height in cm)	14.15	14.35	14.15
$W_{0.5}$ (Width at 50% peak height in cm)	1.40	1.40	1.40
A	0.65	0.65	0.65
B	0.75	0.75	0.75
B/A (Asymmetry ratio)	1.15	1.15	1.15
\overline{M}_2 (Variance in cm^2) ^a	0.47	0.47	0.47
$\overline{X} = 0.47 \text{ cm}^2$			
RSD ^b = 0%			
σ_G (Standard deviation in cm^2)	0.487	0.487	0.487
$\overline{X} = 0.487 \text{ cm}^2$			
RSD = 0%			

a $1 \text{ cm}^2 = 36 \text{ s}^2$.

b Relative standard deviation.

Table VIII. Variance and standard deviation values for pyridoxal in 0.05 M CTAB micellar media at 10% peak height. Variable UV-visible absorbance detector at 292.6 nm, range .1, temperature 45°C, flow rate 1.4 ml/min, tube length 200 cm, i.d. 0.5 mm, 10 μ l sample loop, pyridoxal 2.83×10^{-4} M in 0.05 M CTAB, chart speed 10 cm/min.

h (Peak height in cm)	13.60	13.50	13.70
$w_{0.1}$ (Width at 10% peak height in cm)	2.85	2.90	2.90
A	1.10	1.15	1.15
B	1.75	1.75	1.75
B/A (Asymmetry ratio)	1.59	1.59	1.59
\overline{M}_2 (Variance in cm^2) ^a	0.55	0.55	0.55
$\overline{X} = 0.55 \text{ cm}^2$			
RSD ^b = 0%			
σ_G (Standard deviation in cm^2)	0.445	0.470	0.470
$\overline{X} = 0.462 \text{ cm}^2$			
RSD = 3.12%			

^a 1 $\text{cm}^2 = 36 \text{ s}^2$.

^b Relative standard deviation.

Table IX. Variance and standard deviation values for pyridoxal in 0.05 M CTAB micellar media at 30% peak height. Variable UV-visible absorbance detector at 292.6 nm, range .1, temperature 45°C, flow rate 1.4 ml/min, tube length 200 cm, i.d. 0.5 mm, 10 μ l sample loop, pyridoxal 2.83×10^{-4} M in 0.05 M CTAB, chart speed 10 cm/min.

h (Peak height in cm)	13.60	13.50	13.70
$w_{0.3}$ (Width at 30% peak height in cm)	2.10	2.10	2.10
A	0.95	0.95	0.95
B	1.15	1.15	1.15
B/A (Asymmetry ratio)	1.21	1.21	1.21
\overline{M}_2 (Variance in cm^2) ^a	0.58	0.58	0.58
$\overline{X} = 0.58 \text{ cm}^2$			
RSD ^b = 0%			
σ_G (Standard deviation in cm^2)	0.543	0.543	0.543
$\overline{X} = 0.543 \text{ cm}^2$			
RSD = 0%			

^a 1 $\text{cm}^2 = 36 \text{ s}^2$.

^b Relative standard deviation.

Table X. Variance and standard deviation values for pyridoxal in 0.05 M CTAB micellar media at 50% peak height. Variable UV-visible absorbance detector at 292.6 nm, range .1, temperature 45°C, flow rate 1.4 ml/min, tube length 200 cm, i.d. 0.5 mm, 10 μ l sample loop, pyridoxal 2.83×10^{-4} M in 0.05 M CTAB, chart speed 10 cm/min.

h (Peak height in cm)	13.60	13.50	13.70
$W_{0.5}$ (Width at 50% peak height in cm)	1.60	1.70	1.60
A	0.75	0.80	0.75
B	0.80	0.90	0.85
B/A (Asymmetry ratio)	1.13	1.125	1.13
\overline{M}_2 (Variance in cm^2) ^a	0.59	0.667	0.59
$\overline{X} = 0.616 \text{ cm}^2$			
$\text{RSD}^b = 7.2\%$			
σ_G (Standard deviation in cm^2)	0.566	0.544	0.566
$\overline{X} = 0.559 \text{ cm}^2$			
$\text{RSD} = 2.36\%$			

^a $1 \text{ cm}^2 = 36 \text{ s}^2$.

^b Relative standard deviation.

Table XI. Average values for variance and standard deviation for pyridoxal in 0.05 M CTAB micellar and aqueous media at 10, 30, and 50% peak height for aqueous and 0.05 M CTAB systems.

	10%	30%	50%	\bar{X} (cm^2)	RSD (%)
0.05 M CTAB					
\bar{M}_2 (cm^2)	0.55	0.58	0.616	0.582	5.68
σ_G (cm^2)	0.462	0.559	0.543	0.521	5.20
H_2O					
\bar{M}_2 (cm^2)	0.473	0.559	0.473	0.503	6.06
σ_G (cm^2)	0.448	0.448	0.487	0.461	4.88

exponentially modified Gaussian peak shape. Proven that the FIA peaks in our system were exponentially modified Gaussian, studies of the dispersion in aqueous and micellar system were performed by using equation 4.2. Variance measurements at 10% peak height are more precise than those calculated at 30% and 50% peak height (61).

Given the conditions in Tables V and VIII, the dispersion between aqueous and micellar media was compared in terms of the variance, \bar{M}_2 . The values for \bar{M}_2 were found to be 0.473 and 0.55 cm² for aqueous and 0.05 M CTAB media, respectively.

The dispersion of both aqueous and micellar systems was calculated also by using equation 1.1, which is the definition of FIA dispersion. The concentration of pyridoxal before the dispersion process was measured by passing through the detector a solution of pyridoxal in water (2.81×10^{-4} M) or in 0.05 M CTAB (2.83×10^{-4} M) and measuring the response of the detector. The response of the detector was obtained by the average of six measurements. The concentration of pyridoxal after the dispersion process has taken place was obtained by measuring the maximum peak height of 11 injections of 10 μ l of pyridoxal solutions (above) into pure aqueous or 0.05 M CTAB. Note again that dispersion occurring under this circumstance is only due to physical contributions; no chemical reaction is taking place. The ratio of the detector response before and after the dispersion process occurred was 17.62 for the aqueous system and 19.14 for the micellar system. Contrary to what was expected higher dispersion was found for micellar media. Due to the higher viscosity of 0.05 M CTAB solution compared with water, the dispersion was expected to be less. To prove

the validity of these results, the same type of experiment was performed on two different days and the same results were obtained (see Table XII).

To investigate the effect of surfactant concentration on the dispersion process, a set of dispersion measurements (\bar{M}_2) versus CTAB concentration were performed. The concentration of CTAB was varied from 5×10^{-6} M to 5×10^{-2} M. This range of concentration includes solutions above and below the critical micelle concentration. Ten microliters of pyridoxal (2.81×10^{-4} M) aqueous solution was injected into the stream and from the recorded peaks the variance at 10% peak height was calculated. From Table XIII, one can say that for a solution of 5×10^{-6} M the dispersion obtained is very similar to that calculated for water. Above this concentration an increase in surfactant concentration had no effect on the dispersion up to a concentration of 5×10^{-2} M CTAB, at which point an increase in dispersion was observed. Micellar concentration changes the dispersion of the FIA system. This may be explained by the fact that the pyridoxal molecules are localized on or within the micelle structure. Micellar media is more viscous than aqueous media (43); therefore, the mass transfer in a radial direction decreases. An increase in peak dispersion results because a decrease in mixing across the stream tends to increase dilution of the solute by longitudinal dispersion (42). The increase of dispersion with micellar media needs further study.

Table XII. Dispersion values for aqueous and micellar systems.

	0.05 M CTAB		Aqueous	
	C^0/C^{\max}	\overline{M}_2 (cm^2)	C^0/C^{\max}	\overline{M}_2 (cm^2)
1.	19.54	0.55	17.62	0.47
2.	19.14	0.56	17.05	0.45
3.	19.26	0.54	17.25	0.45

C^0/C^{\max} = ratio of concentration of pyridoxal before and after the dispersion process has taken place.

\overline{M}_2 = variance or second moment in cm^2 .

Table XIII. Measurement of dispersion versus CTAB concentration.
 Variable UV-visible absorbance detector at 292.6 nm,
 range .1, temperature 45°C, flow rate 1.4 ml/min, tube
 length 200 cm, i.d. 0.5 mm, 10 μ l sample loop, pyridoxal
 2.81×10^{-4} M in deionized water, chart speed 10 cm/min.

	\overline{M}_2 (cm^2)	\overline{M}_2 (cm^2)	\overline{M}_2 (cm^2)	\overline{M}_2 Average (cm^2)
CTAB (M)				
5.0×10^{-6}	0.44	0.43	0.46	0.44
2.5×10^{-5}	0.52	0.46	0.52	0.50
5.0×10^{-5}	0.47	0.52	0.49	0.49
2.5×10^{-4}	0.48	0.50	0.46	0.48
5.0×10^{-4}	0.49	0.46	0.52	0.49
2.5×10^{-3}	0.52	0.50	0.49	0.50
5.0×10^{-3}	0.50	0.52	0.52	0.51
2.5×10^{-2}	0.47	0.52	0.49	0.49
5.0×10^{-2}	0.52	0.57	0.53	0.54
H ₂ O	0.43	0.44	0.48	0.45

\overline{M}_2 = variance or second moment in cm^2 .

CHAPTER V CONCLUSIONS AND FUTURE WORK

The applicability of combining the technique of Flow Injection Analysis with micellar catalysis has been shown. The results obtained from the determination of pyridoxal in micellar media compared to those in aqueous media are promising. Higher response, as measured by peak height, was recorded at all times for micellar carrier solutions. Higher sensitivities and lower limits of detection were obtained for the micellar system when the oxidation product of pyridoxal and cyanide was detected either fluorimetrically or by UV absorbance. Higher sensitivity ratios, for micellar to aqueous systems, were obtained when using fluorescence detection. In this case, not only is the reaction taking place at a faster rate but the solubilization of reagents within the micelle structure contributes to increase the signal due to the shielding effect.

With this example, it has been proven that due to the kinetic nature of the FIA technique the use of micellar media can be very advantageous. To support this investigation, the utility of using micellar carrier solution in an FIA system, it will be necessary to perform similar experiments by running different reactions taking place in aqueous and micellar media. Keeping in mind the kind of surfactant that will catalyze the specific reaction (anionic,

cationic, nonionic or zwitterionic), the rate of the reaction should be measured and if it is favorable applied to FIA.

One of the reactions that will be very interesting to look at is the determination of metals by their complexation with dyes in the presence of micelle media (62-68). Some characteristics observed for these metal-dye complexes in micellar media are an increase in molar absorptivity and red shifts in the wavelength of maximum absorbance (63). These substantial changes in the UV visible spectrometry of these complexes together with the technique of FIA can be developed as a new spectrophotometric method for determining micro amounts of metal ions. The resulting method should be fast, easy and inexpensive.

Lower background signals were found for the aqueous systems compared to CTAB micellar systems. Therefore, the limits of detection for micellar media were not as low as expected. This increase in background noise for micellar media needs further study to elucidate if the increase in noise is due to the presence of micelles or if it is just observed with this specific reaction.

Due to the specific interactions between micelles and solutes the selectivity of a particular reaction can be increased, reducing the amount and kind of interferences. An investigation on this topic will be very valuable especially for the determination of very small amounts of analytes.

It has been mentioned that catalysis of organic and inorganic reactions also occur in apolar media in the presence of reversed micelles (19,69). Reversed micelles offer similar and at the same time different characteristics from normal micelles. Future research

on the application of reversed micelles for reactions occurring in apolar media in combination with the technique of FIA will be very interesting.

According to the agreement of the values for the second moment and the standard deviation measured at 10, 30 and 50% peak height, the peaks recorded from an FIA system can be designated to be exponentially modified gaussian.

Higher values for dispersion were found for micellar media. These results were not as expected and need further study to understand better the reason for this increase in dispersion. More detailed experiments should be performed under different conditions, e.g., varying the type and concentration of surfactant, temperature, etc.

The contribution of a chemical reaction to the dispersion of a peak in FIA is not well understood. By comparing the dispersion of different reactions taking place in different types of surfactants to the dispersion obtained in aqueous media could help to explain the contribution of the chemistry to the total dispersion process. The differences in rate of reaction between different micellar and aqueous systems can help to explain this phenomena. By taking a reaction whose rate of reaction varies in the presence of anionic, cationic, nonionic and aqueous media, the contribution of chemical kinetics may be clarified.

REFERENCES

1. Ruzicka, J.; Hansen, E.H. "Flow Injection Analysis"; Wiley-Interscience: New York, 1981.
2. Ruzicka, J.; Hansen, E.H. Anal. Chim. Acta, 1986, 179, 1.
3. Rocks, B.F.; Riley, C. Clin. Chem., 1982, 28, 409.
4. Stewart, K.K. Anal. Chem., 1983, 55, 931A.
5. Ruzicka, J.; Hansen, E.H. Anal. Chim. Acta, 1979, 106, 207.
6. Ranger, C.B. Anal. Chem., 1981, 53, 20A.
7. Ruzicka, J. Anal. Chem., 1983, 55, 1040A.
8. Valcárcel Cases, M.; Luque de Castro, M.D. "Análisis por Inyección en Flujo"; Departamento de Química Analítica, Universidad de Córdoba, Córdoba, 1984.
9. Mottola, H.A. Anal. Chem., 1981, 53, 1312A.
10. Stewart, K.K. Talanta, 1981, 28, 789.
11. Stewart, K.K.; Beecher, G.R.; Hare, P.E. Anal. Biochem., 1976, 70, 167.
12. Ruzicka, J.; Hansen, E.H. Anal. Chim. Acta, 1975, 78, 145.
13. Vanderslice, J.T.; Stewart, K.K.; Rosenfeld, A.G.; Higgs, D.J. Talanta, 1981, 28, 11.
14. Reinj, J.M.; Van Der Linden, W.E.; Poppe, H. Anal. Chim. Acta, 1981, 123, 229.
15. Tijssen, R. Anal. Chim. Acta, 1980, 114, 71.
16. Van Den Berg, J.H.M.; Deeler, R.S.; Egberink, H.G.M. Anal. Chim. Acta, 1980, 114, 91.
17. Ruzicka, J.; Hansen, E.H. Anal. Chim. Acta, 1980, 114, 19.
18. Mittal, K.L., Ed. "Micellization, Solubilization, and Microemulsions"; Plenum Press: New York, 1977; vols. 1 and 2.

19. Lindman, B.; Wennerstrom, H.; Eicke, H.F. "Micelles"; Topics in Current Chemistry No. 87; Springer-Verlag: New York, 1980.
20. Tanford, C. "The Hydrophobic Effect"; 2nd ed.; Wiley-Interscience: New York, 1980.
21. Rossen, M.J. "Surfactants and Interfacial Phenomena"; Wiley-Interscience: New York, 1978.
22. Mittal, K.L.; Fendler, E.J. "Solution Behavior of Surfactants"; Plenum Press: New York, 1982; vols. 1 and 2.
23. Fendler, J.H. "Membrane Mimetic Chemistry"; John Wiley: New York, 1982.
24. Fendler, J.H.; Fendler, E.J. "Catalysis in Micellar and Micromolecular Systems"; Academic Press: New York, 1975.
25. Dill, K.A.; Flory, P.J. Proc. Natl. Acad. Sci. USA, 1981, 78, 676.
26. Berezin, I.V.; Martinek, K.; Yatsimirskii, A.K. Russ. Chem. Rev., 1973, 42, 787.
27. Menger, F.M. Acc. Chem. Res., 1979, 12, 111.
28. Fisher, L.R.; Oakenfull, D.G. Chem. Soc. Rev., 1977, 6, 25.
29. Pelizzetti, E.; Pramauro, E. Anal. Chim. Acta, 1985, 169, 1.
30. Cline-Love, L.J.; Habarta, J.G.; Dorsey, J.G. Anal. Chem., 1984, 56, 1133A.
31. Hinze, W.L. In "Solution Chemistry of Surfactants"; Mittal, K.L., Ed.; Plenum Press: New York, 1979; vol. 1, p. 79.
32. Betteridge, D. Anal. Chem., 1978, 50, 832A.
33. Reijn, J.M.; Van Der Linden, W.E.; Poppe, H. Anal. Chim. Acta, 1981, 126, 1.
34. Reijn, J.M.; Van Der Linden, W.E.; Poppe, H. Anal. Chim. Acta, 1980, 114, 105.
35. Reijn, J.M.; Van Der Linden, W.E.; Poppe, H. Anal. Chim. Acta, 1983, 145, 59.
36. Ruzicka, J.; Hansen, E.H. Anal. Chim. Acta, 1978, 99, 37.
37. Paiton, C.C.; Mottola, H.A. Anal. Chim. Acta, 1984, 158, 67.

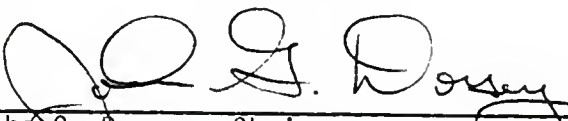
38. Reijn, J.M.; Poppe, H.; Van Der Linden, W.E. Anal. Chem., 1984, 56, 943.
39. Hungerford, J.M.; Christan, G.D.; Ruzicka, J.; Middings, J.C. Anal. Chem., 1985, 57, 1794.
40. Pardue, H.L.; Fields, B. Anal. Chim. Acta, 1981, 124, 39.
41. Pardue, H.L.; Fields, B. Anal. Chim. Acta, 1981, 124, 65.
42. Painton, C.C.; Mottola, H.A. Anal. Chem., 1981, 53, 1713.
43. Cordes, E.H.; Dunlap, R.B. Acc. Chem. Res., 1969, 2, 329.
44. Mittal, K.L.; Lindman, B., Ed. "Surfactant in Solutions"; Plenum Press: New York, 1982; vols. 1 and 2.
45. Cordes, E., Ed. "Reaction Kinetics in Micelles"; Plenum Press: New York, 1973.
46. Abraham, W.; Handler, P.; Smith, E.L.; Stetten, D.W. "Principles of Biochemistry"; McGraw Hill Book Company, Inc.: New York, 1954; pp. 1008-1010.
47. Linares, P.; Luque de Castro, M.D.; Varcárcel, M. Anal. Lett., 1985, 18, 67.
48. Bonavita, V. Arch. Biochem. Biophys., 1960, 88, 366.
49. Oshishi, N.; Fukui, S. Arch. Biochem. Biophys., 1968, 128, 606.
50. Linares, P.; Luque de Castro, M.D.; Varcárcel, M. Anal. Chim. Acta, 1984, 18, 67.
51. Moore, J.W.; Pearsen, R.G. "Kinetics and Mechanism"; Wiley-Interscience: New York, 1981.
52. Hinze, W.L.; Singh, H.N.; Baba, Y.; Harvey, N.G. Trends Anal. Chem., 1984, 3, 193.
53. Turro, N.J.; Grätzel, M.; Braun, A.M. Angew. Chem. Int. Ed. Engl., 1980, 19, 675.
54. Anagnostopoulou, P.I.; Koupparis, M.A. Anal. Chem., 1986, 58, 322.
55. Betteridge, D.; Sly, T.J.; Wade, A.P.; Tillman, J.E. Anal. Chem., 1983, 55, 1292.
56. Burke, G.C.; Stedman, G.; Wade, A.P. Anal. Chim. Acta, 1983, 153, 277.

57. Legett, D.J. J. Chem. Ed., 1983, 60, 707.
58. Shavers, C.L.; Parsons, M.L.; Deming, S.N. J. Chem. Ed., 1979, 56, 307.
59. Buton, C.A.; Wolfe, B. J. Am. Chem. Soc., 1973, 95, 3742.
60. Poppe, H. Anal. Chim. Acta, 1980, 114, 59.
61. Foley, J.P.; Dorsey, J.G. Anal. Chem., 1983, 55, 730.
62. Diaz Garcia, M.E.; Sanz-Medel, A. Talanta, 1986, 33, 255.
63. Callahan, J.H.; Cook, K.D. Anal. Chem., 1984, 56, 1632.
64. Jarosz, M.; Marczenko, Z. Analyst, 1984, 109, 35.
65. Marczenko, Z.; Jarosz, M. Analyst, 1982, 107, 1431.
66. Marczenko, Z.; Kalowska, H. Anal. Chim. Acta, 1981, 123, 279.
67. Xi-Wen, H.; Poe, D.P. Anal. Chim. Acta, 1981, 131, 195.
68. Medina, J.; Hernández, F.; Marin, R.; López, F.J. Analyst, 1986, 111, 235.
69. Fendler, J.H. Acc. Chem. Res., 1976, 9, 153.

BIOGRAPHICAL SKETCH

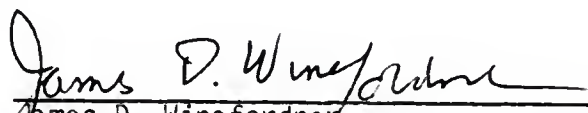
María A. Hernández Torres was born in Mayagüez, Puerto Rico, on May 29, 1958. She received her elementary and high school education at the Colegio de La Milagrosa, Mayagüez, Puerto Rico. In 1980, she completed her Bachelor of Science degree in chemistry at the University of Puerto Rico Mayagüez Campus (magna cum laude). In 1983, she pursued a Master of Science degree in analytical chemistry at the University of Florida. She is now receiving a Doctor of Philosophy degree in analytical chemistry at the University of Florida.

I certify that I have read this study and that in my opinion it conforms to acceptable standards of scholarly presentation and is fully adequate, in scope and quality, as a dissertation for the degree of Doctor of Philosophy.




John G. Dorsey, Chairman
Associate Professor of Chemistry

I certify that I have read this study and that in my opinion it conforms to acceptable standards of scholarly presentation and is fully adequate, in scope and quality, as a dissertation for the degree of Doctor of Philosophy.



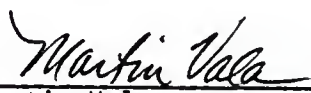
James D. Winefordner
Graduate Research Professor of Chemistry

I certify that I have read this study and that in my opinion it conforms to acceptable standards of scholarly presentation and is fully adequate, in scope and quality, as a dissertation for the degree of Doctor of Philosophy.




Anna F. Brajter-Toth
Assistant Professor of Chemistry

I certify that I have read this study and that in my opinion it conforms to acceptable standards of scholarly presentation and is fully adequate, in scope and quality, as a dissertation for the degree of Doctor of Philosophy.



Martin Vala
Professor of Chemistry

I certify that I have read this study and that in my opinion it conforms to acceptable standards of scholarly presentation and is fully adequate, in scope and quality, as a dissertation for the degree of Doctor of Philosophy.



Christopher M. Riley
Assistant Professor of Pharmacy

This dissertation was submitted to the Graduate Faculty of the Department of Chemistry in the College of Liberal Arts and Sciences and to the Graduate School and was accepted as partial fulfillment of the requirements for the degree of Doctor of Philosophy.

August, 1986

Dean, Graduate School

UNIVERSITY OF FLORIDA



3 1262 08554 1471